Evaporation of freely suspended single droplets: experimental, theoretical and computational simulations

2013 Rep. Prog. Phys. 76 034601

(http://iopscience.iop.org/0034-4885/76/3/034601)

IOP PUBLISHING REPORTS ON PROGRESS IN PHYSICS
Rep. Prog. Phys. **76** (2013) 034601 (19pp) doi:10.1088/0034-4885/76/3/034601

Evaporation of freely suspended single droplets: experimental, theoretical and computational simulations

R Hołyst[1], M Litniewski[1], D Jakubczyk[2], K Kolwas[2], M Kolwas[2], K Kowalski[2], S Migacz[2], S Palesa[2] and M Zientara[2]

[1] Institute of Physical Chemistry of the Polish Academy of Sciences Kasprzaka 44/52, 01-224 Warsaw, Poland
[2] Institute of Physics of the Polish Academy of Sciences al. Lotników 32/46, 02-668 Warsaw, Poland

E-mail: rholyst@ichf.edu.pl and Daniel.Jakubczyk@ifpan.edu.pl

Received 1 December 2011, in final form 29 November 2012
Published 25 February 2013
Online at stacks.iop.org/RoPP/76/034601

Abstract
Evaporation is ubiquitous in nature. This process influences the climate, the formation of clouds, transpiration in plants, the survival of arctic organisms, the efficiency of car engines, the structure of dried materials and many other phenomena. Recent experiments discovered two novel mechanisms accompanying evaporation: temperature discontinuity at the liquid–vapour interface during evaporation and equilibration of pressures in the whole system during evaporation. None of these effects has been predicted previously by existing theories despite the fact that after 130 years of investigation the theory of evaporation was believed to be mature. These two effects call for reanalysis of existing experimental data and such is the goal of this review. In this article we analyse the experimental and the computational simulation data on the droplet evaporation of several different systems: water into its own vapour, water into the air, diethylene glycol into nitrogen and argon into its own vapour. We show that the temperature discontinuity at the liquid–vapour interface discovered by Fang and Ward (1999 *Phys. Rev.* E **59** 417–28) is a rule rather than an exception. We show in computer simulations for a single-component system (argon) that this discontinuity is due to the constraint of momentum/pressure equilibrium during evaporation. For high vapour pressure the temperature is continuous across the liquid–vapour interface, while for small vapour pressures the temperature is discontinuous. The temperature jump at the interface is inversely proportional to the vapour density close to the interface. We have also found that all analysed data are described by the following equation: $\mathrm{d}a/\mathrm{d}t = P_1/(a + P_2)$, where a is the radius of the evaporating droplet, t is time and P_1 and P_2 are two parameters. $P_1 = -\lambda\Delta T/(q_{\mathrm{eff}}\rho_{\mathrm{L}})$, where λ is the thermal conductivity coefficient in the vapour at the interface, ΔT is the temperature difference between the liquid droplet and the vapour far from the interface, q_{eff} is the enthalpy of evaporation per unit mass and ρ_{L} is the liquid density. The P_2 parameter is the kinetic correction proportional to the evaporation coefficient. $P_2 = 0$ only in the absence of temperature discontinuity at the interface. We discuss various models and problems in the determination of the evaporation coefficient and discuss evaporation scenarios in the case of single- and multi-component systems.

(Some figures may appear in colour only in the online journal)

Contents

1. Introduction

Evaporation is a process ubiquitous in nature [1] and technology [2]. This process influences not only the climate [1, 3, 4], the formation of clouds [5], transpiration in plants [6], the survival of arctic organisms [7], the efficiency of car engines [8], but also the structures of dried materials [9–11]. Solar radiation is not completely absorbed by the Earth's atmosphere—the ocean's surface collects most of the incoming solar radiation. Thus solar radiation provides energy for water evaporation. Water evaporation has a tremendous impact on global warming, because water is the main greenhouse gas in the atmosphere [1, 3]. Even though there is a small triggering by CO_2, which initially influences the tropospheric temperature increase, the subsequent moistening of the atmosphere by water vapour is considered by many to be an important feedback mechanism [12]. Fuel evaporation in combustion engines is another process whose efficiency determines the fuel consumption of car engines [2, 8].

Models and theories of evaporation have been developed for over 100 years, but experimental studies have lagged behind the theory. Our knowledge about the dynamic pathway of this phase transition is limited and largely based on speculations rather than on solid experimental facts or computer simulations. Irreversible pathways between equilibrium states are not well understood. Less is known about general rules, which govern systems far from equilibrium. Even in the old fields of irreversible thermodynamics there is plenty to be discovered. On the other hand, experiments encountered problems in the determination of spatial and temporal profiles of thermodynamic parameters during evaporation including the precise measurement of vapour pressure at the micrometre/micrometre length scales. In 1999 Ward and coworkers [13] performed experiments of water evaporation and determined the temperature profile of water and its vapour during evaporation. The temperature of the evaporating liquid (water) was close to the triple point and consequently the vapour pressure was low. Therefore the mean free path in the vapour was large (from 9 to 25 μm). Special small thermocouples were used [13] to measure the temperature profile with spatial resolution of the order of one mean free path in the vapour, i.e. $\sim$10 μm. The temperature profile exhibited an unexpected jump at the interface with the vapour temperature being larger by approximately 10 K than the liquid temperature. This liquid–vapour temperature difference at the interface [13] was opposite in sign to the one predicted by the kinetic theories [14–18]. The theory predicted temperatures smaller in the vapour than in the liquid. For the experimental conditions of Fang and Ward [13] the classical kinetic theory predicted a temperature jump of 0.007 K [19]. Thus the theoretical prediction was three orders of magnitude too small and, moreover, in the opposite direction. This result was surprising because the theory of evaporation was considered to be mature after more than 100 years of study [20]. Ward and coworkers further investigated the problem [21] and concluded that in other substances a substantial temperature jump at the interface also occurs. Theoretical studies of the effect followed the experimental studies [22] to explain the phenomenon, including the statistical rate theory (SRT) for evaporation [23]. Two main effects were considered as a source of the jump: energy flux across the vapour and the difference between the vapour pressure during evaporation and the actual saturation pressure at the liquid temperature. The transport of energy across the vapour phase was not considered in classical theories as a rate limiting step of evaporation [22, 24]. In classical theories more emphasis was put on the mass transport from the interface by diffusion or kinetic-limited motion.

Another surprising result, related to pressure profiles during evaporation, came from computer simulations of evaporating droplets of Lennard-Jones fluids [25–27]. The simulations followed the solutions of the equations of the irreversible thermodynamics in the two phase region during evaporation of argon droplets [28, 29]. Irreversible thermodynamics studies predicted [28] that pressures are equal in the vapour phase everywhere and satisfy the Laplace law for the evaporating droplet. This observation of momentum/pressure equilibrium during evaporation was overlooked in all previous theoretical studies. The solution of the equations of irreversible thermodynamics was obtained for a system 1 μm in size, heated at the boundaries, with a 60 nm droplet evaporating in the middle of the spherical container. The study also indicated that the main process limiting evaporation was the transport of energy across the vapour. Due to numerical problems, the study was limited to high vapour densities close to the critical point. The ratio of the liquid density to the vapour density was at most 10. The results were tested in computer simulations of the Lennard-Jones fluid [25] further away from the critical point with the density ratio as high as 100.

The computer simulations confirmed that during evaporation the momentum/pressure equilibrium is satisfied and the Laplace law obeyed in the process even for nanoscopic droplets (here the system size was 90 nm with a 9 nm droplet). Mechanical equilibrium was further confirmed in the evaporation of bi- and triatomic Lennard-Jones liquids [27]. The most spectacular manifestation of momentum/pressure equilibrium during evaporation was found in the computer simulations of evaporation into the vacuum. In this case the momentum flux of the evaporating liquid exactly matched the liquid pressure setting 'mechanical equilibrium' in these extreme conditions of evaporation [26, 27]. Mechanical equilibrium means that at every point of the system the net force is zero. At equilibrium this condition means equality of pressure at every part of the system. In non-equilibrium processes a net momentum flux should be matched by the pressure, e.g. for evaporation into the vacuum the momentum flux from the flat interface is equal to the pressure inside the evaporating liquid. Computer simulations [25] also showed that for low vapour pressure the temperature at the interface jumps as in the experiments of Fang and Ward [13]. The temperature jump was as high as 30 K, but decreased to zero for higher vapour pressures in accordance with the solutions of the equations of irreversible thermodynamics close to the critical point [28]. During the last decade previous classical theories of evaporation based on the detailed study of mass transport have been questioned on the basis of these new results: the temperature jump at the interface and momentum/pressure equilibrium during evaporation. Although we still wait for precise measurements which would confirm momentum/pressure equilibrium during evaporation, already Ward and Stanga [30] have noticed that during evaporation the vapour pressure was close to the saturation pressure at the liquid temperature—indicating indirectly the momentum/pressure equilibrium in the system.

None of these effects have been fully incorporated into the models of evaporation so far and therefore our current understanding of evaporation needs deep revisions. In this paper we perform a combined analysis of experimental and computational simulation data to address the aforementioned issues. The data concern: evaporation of liquids (water and argon) into its own vapour and evaporation of water and glycol into air or nitrogen atmosphere. We concentrate our attention on the description of a particularly simple system for analysis: a single freely suspended droplet. We present a phenomenological equation describing the radius of the droplet as a function of time and analyse this equation. We show that the phenomenological equation is valid in all studied cases. The continuous description based on the irreversible thermodynamics is presented and two major approximate models are given. One, which follows the original work of Maxwell is concentrated on the mass diffusion in vapour as the rate limiting step for evaporation. The second model is based on the transport of heat across the vapour. We discuss how both models fit the data. Additionally we show that in most cases there are kinetic corrections to the existing data. We show in computer simulations that kinetic corrections appear when there is a temperature jump at the interface. In particular we show that, in order to fully explain evaporation, a detailed analysis of the temperature, density and pressure profiles during evaporation is needed. The analysis of the mass flux only is not sufficient to discern between different theories. We leave the problem of the momentum/pressure equilibrium as a constraint in evaporation theories open, although we explain qualitatively how momentum/pressure equilibrium affects the temperature jump at the interface.

The paper is organized as follows: In section 4 we discuss the details of the experiments on evaporation of droplets trapped in electric fields. In section 2 we discuss the hydrodynamic models for evaporation, the kinetic models and corrections to the continuous description. Section 3 is devoted to the discussion of evaporation coefficients and the influence of impurities in a droplet upon evaporation. In section 5 we fit two different models to the experimental data. One model assumes that evaporation is limited by the diffusive mass transfer from the interface while the second model assumes that the rate limiting factor is heat transfer through the vapour to the surface of the evaporating droplet. We also discuss SRT theory applied to the evaporation of water into its own vapour and into the nearly saturated water/nitrogen vapour. Section 6 presents a comparison between the theory discussed in the previous section and the computational simulations of evaporating droplets of argon at the nanoscale. The detailed analysis of finite size effects shows how to re-scale the simulation parameters to compare the model and the experiments at the microscale to the nanoscale simulations correctly. Section 7 contains the conclusions and discussion.

2. The evaporation model based on the Maxwell description

The problem of the stationary evaporation of a free, spherical, motionless droplet of a pure liquid in an infinite, inert medium was first addressed by Maxwell [31]. His description, based on mass and heat conservation equations, is still widely utilized and considered generally adequate. A general equation of mass conservation for a spherically symmetric system may take the following form [32] (compare e.g. [33]):

$$\frac{\partial}{\partial t}\left(\rho r^2 Y_i\right) = \frac{\partial}{\partial r}\left(\rho r^2 D \frac{\partial Y_i}{\partial r}\right) - \frac{\partial}{\partial r}\left(\rho u r^2 Y_i\right), \qquad (1)$$

where r is the distance from the droplet centre, ρ is the total density of the gaseous environment, Y_i is the mass fraction of component i (for a two-component system: $Y_{\mathrm{vap}} + Y_{\mathrm{air}} = 1$, $\partial Y_{\mathrm{vap}}/\partial r = -\partial Y_{\mathrm{air}}/\partial r$; one component: $Y_{\mathrm{vap}} \equiv 1$, $\partial Y_{\mathrm{vap}}/\partial r \equiv 0$), D is the gas-phase (mutual) diffusion coefficient and u is the flow (radial) velocity. In the case of an evaporating droplet u is relative to the regressing surface. The significance of various processes that (1) encompasses varies substantially against the system's composition and thermodynamic conditions. We shall try to address this issue.

While the analysis of transient processes during combustion may require consideration of the time derivative, (quasi) stationary evaporation enables its omission. The so-called 'moving boundary' effect [34] is automatically lost when the time derivative is dropped. For stationary but fast

evaporation, it should and may be accounted for by other means.

The mass balance at the interface requires that the steady state vapour mass flux described with (1) equals to the evaporation rate of the droplet $a^2\dot{a}\rho_{\mathrm{L}}$, where ρ_{L} is the density of liquid and $\dot{a} \equiv \mathrm{d}a/\mathrm{d}t$. The non-evaporating component is obviously not transported across the interface (the solubility of gases in liquids is neglected here). In compact form these conditions can be expressed as:

$$\rho r^2 D\frac{\partial Y_i}{\partial r} - \rho u r^2 Y_i = -a^2\dot{a}\rho_{\mathrm{L}}\delta_{i\,\mathrm{vap}}, \tag{2}$$

where $\delta_{i\,\mathrm{vap}}$ is the Kronecker delta. It is worth noting that the equation of continuity for the whole system takes then a simple form:

$$\rho u r^2 = a^2\dot{a}\rho_{\mathrm{L}}. \tag{3}$$

For a two-component system, (2) for a non-evaporating component can easily be identified as the definition of Stefan flow. This flow plays an important role only for a limited range of thermodynamic conditions: partial vapour pressure must be at least comparable to the partial pressure of the remaining gas. For a water droplet under atmospheric conditions Stefan flow constitutes a correction to the diffusive flow of only ∼1%. For slowly evaporating DEG it is even smaller. Then u can be set to zero. The solution of (2) under such an approximation will be discussed later on.

Under the assumption of stationary evaporation, ideal gas (density related to temperature via an equation of state) and constant ρD, (1) can be easily integrated. It is convenient to write down the resulting equation in a form describing the evolution of the droplet radius (compare [35]):

$$\dot{a} = -\frac{\rho D}{\rho_{\mathrm{L}} a}\ln\left[\left(1 - \frac{MT_\infty}{M_{\mathrm{air}}T_{\mathrm{L}}}\frac{p_a(T_{\mathrm{L}})}{p}\right)\Big/\left(1 - \frac{M}{M_{\mathrm{air}}}\frac{p_\infty}{p}\right)\right], \tag{4}$$

where a stands for the droplet radius, T_∞ and T_{L} are temperatures far from the droplet and at the droplet surface in the liquid phase, respectively, p, p_a and p_∞ are the total pressure of the gaseous environment, the partial vapour pressure at the droplet, surface and the partial vapour pressure far from the droplet, respectively, M is the molecular mass of the liquid/vapour and M_{air} is the effective molecular mass of the ambient gas. It has been pointed out [36] that a strictly applied boundary condition would require T_{L} on the gas side of the interface (see (10)). However, a temperature discontinuity is encountered there [13, 36], and thus, such an attitude may introduce significant errors. In general ρD depends on the temperature profile $T(r)$ and if necessary should be integrated accordingly. For large droplets down to several micrometres, $p_a \simeq p_{\mathrm{sat}}$, the equilibrium (saturation) vapour pressure at a given temperature. However, if the droplet is relatively small the effects of the surface tension must also be accounted for. Then, the equilibrium vapour pressure above the interface of radius a is expressed by the Kelvin equation (see e.g. [37]):

$$p_a(T_{\mathrm{L}}) = p_{\mathrm{sat}}(T_{\mathrm{L}})\exp\left(\frac{M}{RT_{\mathrm{L}}\rho_{\mathrm{L}}}\frac{2\gamma}{a}\right), \tag{5}$$

where γ is the surface tension of the liquid and R is the universal gas constant. The possible effects of the droplet charge are negligible for micrometre-sized droplets and the effects of impurities present in real liquids will be discussed later on.

In the case of $MT_\infty p_a(T_{\mathrm{L}}) \ll M_{\mathrm{air}}T_{\mathrm{L}}p$ (negligible Stefan flow in a two-component system), (4) reduces to the Maxwell equation:

$$\dot{a} = \frac{MD}{aR\rho_{\mathrm{L}}}\left[\frac{p_\infty}{T_\infty} - \frac{p_a(T_{\mathrm{L}})}{T_{\mathrm{L}}}\right]. \tag{6}$$

For low-volatility liquids under standard conditions, several micrometre-sized droplets (surface tension energy is negligible) and an infinite gaseous medium initially void of vapour, the evaporation can be described with an ultimately simple diffusive mass transport equation [38, 39],

$$\dot{a} = -\frac{D}{\rho_{\mathrm{L}}a}\frac{Mp_{\mathrm{sat}}(T_{\mathrm{L}})}{RT_{\mathrm{L}}}. \tag{7}$$

For a one-component system (e.g. a droplet of argon, modelled by a Lennard-Jones liquid see e.g. [40, 41], evaporating into its own vapour), (2) degenerates into (3). As a consequence u cannot be neglected though it does not fall within the definition of Stefan flow. Moreover, it becomes obvious that the only possible gradient of ρ is caused by the gradient of T. Then, one-component evaporation should be described with the equation of transport of heat and equations (4), (6) and (7) are out of place, since the mutual diffusion cannot be simply replaced by self-diffusion.

As the evaporation taking place at the droplet's surface is associated with the change of enthalpy (latent heat) the equation of the transport of mass must be, in general, accompanied by the equation of the transport of heat. The appropriate fluid dynamics equation for energy transport in a gaseous medium in a reasonably general form is [32]:

$$\frac{\partial}{\partial t}\left(\rho r^2 h\right) = \frac{\partial}{\partial r}\left(\rho r^2 D\sum_i h_i\frac{\partial Y_i}{\partial r}\right) + \frac{\partial}{\partial r}\left(\lambda r^2\frac{\partial T}{\partial r}\right) - \frac{\partial}{\partial r}\left(\rho u r^2 h\right) + r^2\frac{\partial p}{\partial t}, \tag{8}$$

where λ is the thermal conductivity of the gaseous medium, h, h_{vap} and h_{air} are enthalpies of compound gaseous medium, vapour and air, respectively; $h = c_P(T - T_\infty)$ where c_P, being the specific heat capacity under constant pressure, was assumed constant within the range of temperatures concerned.

Again, for quasi-stationary processes the time derivatives may be dropped and the steady state transport of heat for either a one- or two-component system can be described with the following concise equation:

$$\frac{\partial}{\partial r}\left[\rho r^2 D\left(h_{\mathrm{vap}} - h_{\mathrm{air}}\right)\frac{\partial Y_{\mathrm{vap}}}{\partial r}\right] + \frac{\partial}{\partial r}\left(\lambda r^2\frac{\partial T}{\partial r}\right) - \frac{\partial}{\partial r}\left(\rho u r^2 h\right) = 0. \tag{9}$$

The heat transported in a gaseous medium, described with the above equation, is balanced at the interface by the heat

transported from the liquid phase and the heat needed for vaporizing liquid at the surface:

$$\lambda a^2 \left.\frac{\partial T}{\partial r}\right|_{r\to a(+)} = \lambda_{\mathrm{L}} a^2 \left.\frac{\partial T}{\partial r}\right|_{r\to a(-)} + a^2 \dot{a}\rho_{\mathrm{L}} q_{\mathrm{eff}}, \qquad (10)$$

where λ_{L} is the thermal conductivity of the liquid medium and q_{eff} is the effective enthalpy of vaporization (per unit mass). The 'effective value' approach is adopted since the enthalpy of vaporization is defined and measured for equilibrium conditions, while droplet evaporation may be quite far from equilibrium. It is usually assumed, and we follow this scheme here, that the transport of heat in the liquid phase is negligible and T_{L} is uniform in the liquid, though in general there may also be a considerable temperature gradient in the droplet.

Combining equations (9) and (10) under the assumption of instantaneous evaporation (no heat consumption from the liquid phase) and the constant c_P leads to a more general expression than (4) (compare e.g. [40, 41]):

$$\dot{a} = -\frac{\lambda}{a\rho_{\mathrm{L}} c_P} \ln\left[1 + \frac{c_P\,(T_\infty - T_{\mathrm{L}})}{q_{\mathrm{eff}}}\right]. \qquad (11)$$

It is worth noticing that in many cases the transfer of heat by conductivity and by diffusion is comparable. The relative importance of these two modes is characterized by the Lewis number $Le = (\lambda/c_P)/(\rho D)$. In the case of argon droplets evaporating into their own vapour $Le \simeq 1$ with good accuracy (compare LJ simulations below; again, D is self-diffusion). For water droplets in air under standard conditions $Le \simeq 1.16$. For droplets of DEG under similar conditions $Le \gg 1$. $Le = 1$ is a readily made approximation in order to obtain formulae of the (11) type. However, for both one- and two-component systems (11) can be derived without such an approximation and so is valid for any Le as far as c_P is constant.

Again, under the assumption of $c_P(T_\infty - T_{\mathrm{L}}) \ll q_{\mathrm{eff}}$, (11) takes the form:

$$\dot{a} = -\frac{\lambda}{a q_{\mathrm{eff}}\rho_{\mathrm{L}}}\,[T_\infty - T_{\mathrm{L}}(t)] \qquad (12)$$

or

$$\dot{a} = -\frac{\rho D c_P}{a q_{\mathrm{eff}}\rho_{\mathrm{L}}}\,[T_\infty - T_{\mathrm{L}}(t)]$$

for $Le = 1$. It is worth noting that in the case of slow, quasi-isothermal evaporation ($T_\infty - T_{\mathrm{L}}(t) < 0.1$ K), the coupling of equations (4) and (11) (as well as for their simplified forms) via T_{L} can be neglected, and they can be used independently. We can also use the enthalpy of vaporization measured at equilibrium $q_{\mathrm{eff}} = q$.

2.1. Kinetic effects

The equations of fluid dynamics do not hold where the gradients of described quantities are high [33]. In particular, the fluid dynamics description of droplet evaporation assumes continuity of temperature across the interface. Close to the critical point, it seems adequate (as was shown for LJ e.g. in [25]) but generally is not the case [13, 36]. Similarly, a high gradient of vapour density close to the surface must be considered [42].

The evaporation in the region below the mean free path of the gas molecule from the surface is treated as kinetic-limited [43] and thus governed by the Hertz–Knudsen–Langmuir (HKL) equation. For a droplet in vacuum it takes the following form (compare [44]):

$$\dot{a} = -\frac{\alpha_{\mathrm{C}}}{\rho_{\mathrm{L}}}\frac{p_{\mathrm{sat}}(T_{\mathrm{L}})}{\sqrt{2\pi k T_{\mathrm{L}}}}\sqrt{m}, \qquad (13)$$

where m is the mass of a molecule, k is the Boltzmann constant and α_{C} is the evaporation coefficient. This coefficient, defined as the probability of the crossing of the interface by a molecule impinging on it, was introduced by Knudsen [45] to reconcile the experimental findings with the predictions of the theory. The experimentally observed evaporation rate in the kinetic regime is never greater than theoretically allowed by the kinetic theory of gases. Although conceptually seemingly simple, this coefficient turned out to be quite difficult to measure. There is a barrier at the gas–liquid interface, although its nature has not been thoroughly understood yet (see e.g. [46–49]). The issue of evaporation into vacuum, also essential for understanding the kinetics at the gas–liquid interface, has not been satisfactorily resolved yet (see e.g. [26, 50–53]), however it seems that the application of the HKL equation in its standard form may not be adequate in that case. An especially unexpected result is presented in [26]. The flux of evaporation of an LJ liquid into vacuum, obtained from MD calculations, was reproduced with the HKL equation where stagnation temperature was used for T_{L}. Here $\alpha_{\mathrm{C}} = 2$. Such value of this factor indicates that it cannot be interpreted straightforwardly as the evaporation coefficient, which is defined in terms of a probability smaller than or equal to 1 [45].

It is a standard practice [35, 38] to write a single equation accounting both for diffusive and kinetic-limited transport. It is usually done by matching equations (6) and (13) at the distance from the droplet Δ_{C} where the diffusive and kinetic-limited fluxes balance. Δ_{C} is comparable with the mean free path of particles of the surrounding gaseous medium l_a, although its exact value is rather arbitrary (compare [38]), which obscures the physical sense of the resulting equation (e.g [38, 54]). It must be also kept in mind that repeating this procedure for equations (4) and (11) (accounting for the Stefan flow) would lead to slightly different formulae.

In our works we have followed [35, 38] and used (6), with D substituted by an effective diffusion coefficient taking into account the kinetic effects

$$D_k(a, T_{\mathrm{L}}) = \frac{D}{a/(a+\Delta_{\mathrm{C}}) + D\sqrt{2\pi M/(RT_{\mathrm{L}})}/(a\alpha_{\mathrm{C}})}. \qquad (14)$$

It should be highlighted that in order to arrive at (14) a further approximation of $T_{\mathrm{L}} = T(a + \Delta_{\mathrm{C}})$ is made. It manifests as an overestimation of α_{C} for higher $T_\infty - T_{\mathrm{L}}$ (>0.3 K for water). Trying to avoid this approximation excessively complicates calculations. However, it is possible to partially correct the value of α_{C} afterwards, using the formula developed in [43].

Similarly, the effective thermal conductivity (with kinetic effects included) of ambient gas (moist nitrogen/air for experiments with water in [43]) may be expressed as follows (and used in (12) instead of λ):

$$\lambda_k(a, T_L) = \frac{\lambda}{a/(a+\Delta_T) + \lambda\sqrt{2\pi M_{air}/(RT_L)}/(a\alpha_T \rho c_P)}, \tag{15}$$

where Δ_T and α_T (the thermal accommodation coefficient) play roles analogous to Δ_C and α_C, respectively.

Two characteristic length scales can be identified in each of the above formulae: Δ_C and $4D/(\alpha_C \overline{v})$ in (14) and Δ_T and $4\lambda/(\alpha_T \rho c_P \overline{v_{air}})$ in (15), where $\overline{v}$ and $\overline{v_{air}}$ are the average thermal velocity of vapour and ambient gas molecules, respectively. However, it is worth noticing that

$$\frac{\Delta_C}{4D/(\alpha_C \overline{v})} \simeq \frac{3\alpha_C D^*}{4D} \quad \text{and} \quad \frac{\Delta_T}{4\lambda/(\alpha_T \rho c_P \overline{v_{air}})} \simeq \frac{3\alpha_T}{4Le}, \tag{16}$$

where D^* is the coefficient of self-diffusion of vapour and the Lewis number is associated with self-diffusion in ambient gas. Thus, the two length scales are linked and furthermore Δ_C and Δ_T are usually (significantly) smaller. As a consequence, a single, longer length scale a_C can be used and the dimensionless droplet radius κ can be introduced as follows:

$$\kappa = \frac{a}{a_C} = \frac{a}{4D/(\alpha_C \overline{v})} \quad \text{or} \quad \kappa = \frac{a}{a_C} = \frac{a}{4\lambda/(\alpha_T \rho c_P \overline{v_{air}})}, \tag{17}$$

respectively.

For $\Delta_C = \Delta_T \simeq 0$ (see (19) and (21) in section 5) $D_k(a)/D = \lambda_k(a)/\lambda$. The magnitude of D_k and λ_k normalized to D and λ for $\Delta_C = \Delta_T = 0$ is presented in figure 1 versus both a and κ. It can be seen that for a dimensionless droplet of radius $1 \lesssim \kappa \lesssim 5$ (water droplet shrinking from ∼6 to ∼1 μm) under standard temperature and pressure (STP) conditions, the influence of kinetic effects upon the evaporation is clearly recognizable but not dominating.

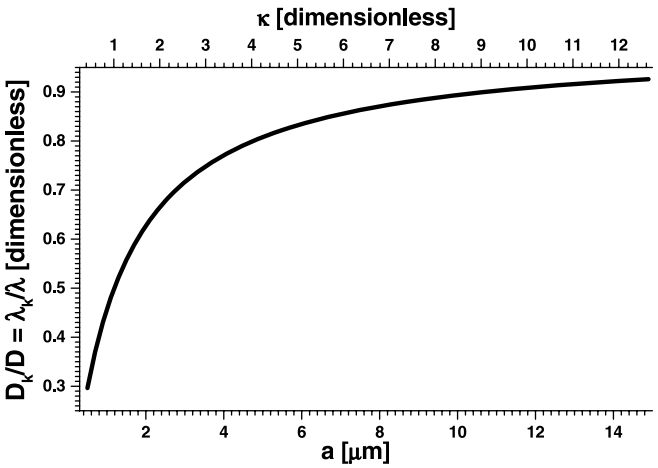

Figure 1. Effective diffusion and thermal conductivity coefficients D_k and λ_k normalized to D and λ, respectively, presented versus droplet radius, both in dimensional form a and dimensionless form $\kappa = a/a_C$, where the characteristic length scale $a_C = 1.18\,\mu$m (see definition (17) and compare with section 5). It should be pointed out that for $a \ll \Delta_C, \Delta_T$ $D_k/D = \lambda_k/\lambda \to \kappa$. The calculation was performed for the conditions when $D_k(a)/D = \lambda_k(a)/\lambda$, corresponding to data presented in figure 6: water droplets in nitrogen atmosphere, 20 °C, 998 hPa, $\alpha_C = 0.14$, $\alpha_T = 0.15$.

3. Discussion of evaporation coefficient issues

Many attempts have been made over nearly a century to determine the values of α_C and α_T experimentally. Most of the experiments considered water and a variety of experimental methods were used. Both condensation on and evaporation from the surface of bulk liquid, liquid films, jets and droplets were investigated in various environments (vacuum, standard air, passive or reactive atmospheres) under various pressures and for various water vapour saturations. Small droplets, such as encountered in clouds, have been favoured since kinetic effects manifest strongly for them. Suspended droplets, trains of droplets, clouds of droplets and single trapped droplets were studied. The results obtained by different authors spanned from ∼0.001 to 1 for α_C and from ∼0.5 to 1 for α_T (see e.g. [34, 55–62] and [38, 63–66] for reviews). There seems to be a better agreement about the value of α_T. The measurements for other vapour–liquid systems are fewer and similarly non-conclusive. Adsorption of heterogeneous vapours on liquid water seems to attract more attention (see [67–72] and [73] for reviews) than single-component evaporation/condensation (see [35] and references therein, and [49, 74–76]). The results seem to suggest that a low evaporation coefficient corresponding to a high interfacial barrier is not unique for water [46, 72].

Experiments with evaporation of polar liquids into vacuum (see e.g. [48] for unsteady state evaporation or [77] for jet stream tensimeter experiments and references in [65, 78]) yield higher values of α_C than (quasi) equilibrium experiments [43, 66, 79]. On the other hand, much lower values of α_C at 300 K can be found in [76] and the works cited therein. In those studies, a so-called dropwise condensation method was used (compare [61] for water). This method yields $\alpha_C \simeq 0.4$ at atmospheric pressure and $\alpha_C \to 0.2$ for $p \to 0$.

The measurement of temperature dependence of α_C or α_T was rarely attempted and the results were inconclusive. Recent studies for water by Li *et al* [55] and by Winkler *et al* [54] (see [66] for comparison of these studies) can serve as an example. The authors of the first study (Boston College/Aerodyne Research Inc. group) found that α_C decreases with temperature within the temperature range between 257 and 280 K. The authors of the second study (University of Vienna/University of Helsinki group) claim that α_C and α_T exhibit no temperature dependence between 250 and 290 K. Our results for water versus temperature [43] are in excellent agreement with those obtained with a fundamentally different method of the BC/ARI group. On the other hand, our modelling and the modelling of the UV/UH group seems to differ only by second order effects, while the results differ significantly. What, in our opinion, makes a fundamental difference can be seen in the data from [54]. They exhibit a strictly linear $a^2(t)$ dependence (the so-called D^2-law, see e.g. formula (32)) which signifies that, quite unexpectedly, the kinetic effects do not manifest

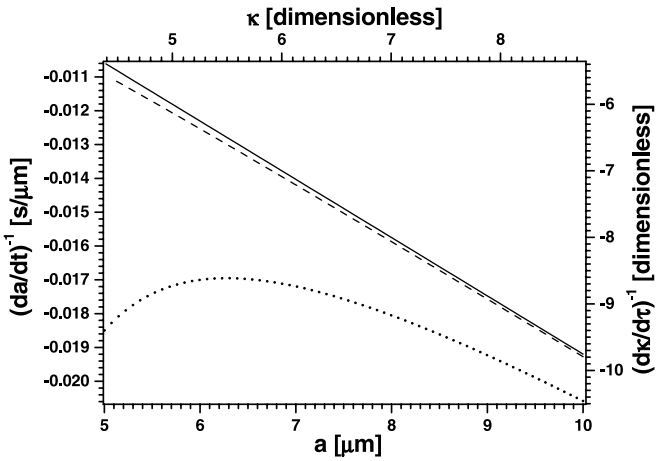

Figure 2. Estimation of the effect of impurities (n_s constant is proportional to the initial mass fraction of impurities) upon droplet radius evolution for water droplets evaporating into dry nitrogen under STP conditions. Dimensionless coordinates $\kappa = a/a_C$ and $d\kappa/d\tau = \dot{a}t_C/a_C$, where $a_C = 1.14\,\mu$m and $t_C = 2.2$ ms. Solid line—no impurities; dashed line—a small amount of impurities ($n_s \simeq 5 \times 10^{-5}$); dotted line—a considerable amount of impurities ($n_s \simeq 1 \times 10^{-3}$).

strongly. This probably led to an overestimation of α_C. All these experiments show that finding a reliable value of α_C is a difficult task.

3.1. The obscuring effect of impurities

Although in this work we essentially deal with pure liquids, real liquids used in experiments always contain some impurities. Real liquids may be (and usually are) simultaneously contaminated with substances of higher and lower volatility, as well as with non-volatile substances and insoluble particles. Although, in our experiments, we took great care to avoid impurities and their effects, the mode of their influence upon the observed droplet evolutions must be kept in mind. The presence of low-volatility (or non-volatile) impurities can be easily observed in both figures (4) and (5) as well as in figure 6. In figure 4 it manifests as a 'kink' at the end of the evolution, which, after differentiation appears as a dramatic fall in figures (5) and (6). We estimated the effect of impurities for water droplets evaporating into dry nitrogen under conditions corresponding to the data presented in figure 6. The simplest model of the influence of an ideally soluble, non-surface-active, non-volatile impurity was used: the Kelvin (5) was substituted with the Köhler equation (compare [37, 38]):

$$p_a(T_L) = p_{sat}(T_L) \exp\left(\frac{M}{RT_L\rho_L}\frac{2\gamma}{a} - \frac{n_s}{(a/a_0)^3 - n_s}\right), \quad (18)$$

where a_0 is the initial droplet radius and n_s is approximately equal to the initial mass fraction of impurities. We used the set of equations (6), (12), (14) and (15) together with (18) for modelling. The dependence of the quantities and parameters upon temperature was also taken into account. Due to the extreme simplicity of the model the visualization presented in figure 2 is qualitative.

For higher impurity concentration, their influence is significant and highly non-linear. Although the 'kink' (the lowest trace in figure 2) can be easily isolated and avoided, the evolution is visibly slower even in the diffusion regime. This additional slant and shift is noticeable even for a seemingly small concentration of impurities. If not accounted for, it will mask the values of both the diffusion and the evaporation coefficients: the diffusion coefficient would seem lower and the evaporation coefficient higher (see [80] for details).

4. Experimental apparatus and data processing procedures

Our experimental technique is a specific variation of well-established thermogravimetry (see e.g. [81, 82]), under stationary atmosphere and stationary thermodynamic conditions. We used an electrodynamic quadrupole trap (compare e.g. [61, 83–86]) as a balance and a trapped droplet as a sample. The sample/droplet mass evolution was obtained, with $\sim 10^{-3}$ accuracy, from the droplet radius evolution (see below). The outline of the experimental setup as well as the electrodynamic trap is presented in figure 3. The trap was kept in a small ($\sim 10\,cm^3$) thermostatic chamber. Droplets were injected into the trap through the top port. The injector was kept inside the chamber ensuring that the initial temperature of the droplet was equal to that of the chamber. The initial droplet radius was $\sim 10\,\mu$m. Usually we were able to follow the evolution of the radius (in time) for a few micrometres. Before the injection of each droplet, the chamber (and trap) was purged with filtered (H14 grade filter), dry nitrogen obtained by vaporizing liquid nitrogen.

In the case of experiments with water droplets, the chamber was then filled with saturated water vapour/nitrogen mixture, obtained by bubbling dry nitrogen through liquid water. The humidity in the chamber, but outside of the trap, was tentatively monitored with semiconductor sensors. Settling time was allowed for equilibration before the measurements, since the movement of gas with respect to the droplet speeds up the evaporation of larger droplets. This phenomenon is actually utilized in standard thermogravimetry. In the case of experiments with diethylene glycol (DEG), we could not fully avoid the ubiquitous water vapour diffusing from the elements of the chamber and the trap. But, at the timescale of several minutes, the effect of water vapour could be neglected (relative humidity <5%). On the other hand, during experiments with water droplets we could not be sure of water vapour saturation in the chamber due to the condensation on the walls, mainly during filling of the chamber. Complete evaporation of a droplet several micrometres in radius, in our void chamber, would give rise to a vapour pressure several orders of magnitude below the corresponding equilibrium vapour pressure. Thus, the presence of even several droplets did not influence the thermodynamic conditions in the chamber. However, lost droplets can get into the tight spaces of the trap, which after some accumulation can distort the trapping field. In order to avoid this distortion, the trap and the chamber were purged with compressed gas every few hundred injections and dismantled and thoroughly cleaned every several hundred injections.

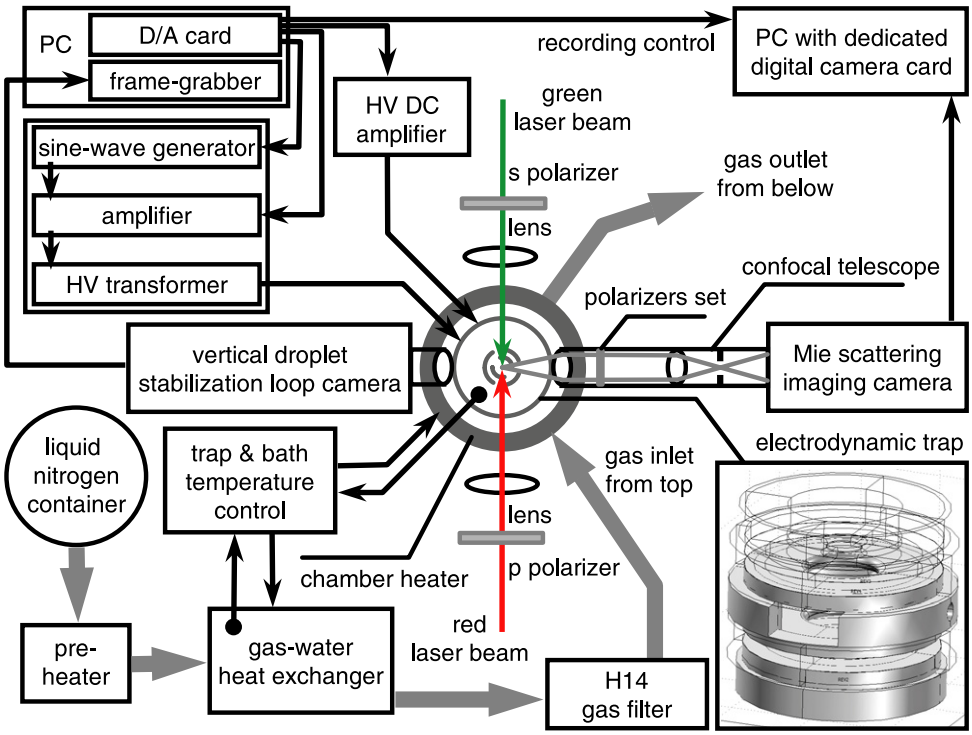

Figure 3. Schematic view of the experimental setup (top view: droplet injector omitted). Inset: electrodynamic trap drawing (wire-frame partially rendered).

In our experiments with DEG we used diethylene glycol 99.99% (BioUltra, GC, Fluka) (purity for the lot stated in GC area % by the manufacturer). For the experiments with water, we used ultra-pure water produced in the lab (Milli-Q Plus, Millipore, resistivity ∼18 MΩ cm, total dissolved solids <20 ppb, total organic carbon (TOC) ⩽10 ppb, no suspended particles larger than 0.22 μm, microorganisms ⩽1 colony forming unit per ml, silicates <0.1 ppb and heavy metals ⩽1 ppb). All liquids were transferred into the droplet injector with due care and without delay. The experiment was conducted within one hour of the transfer. The effects (ionic dissolving, chemical reactions) caused e.g. by atmospheric CO_2 were avoided by substituting air with nitrogen in the climatic chamber.

The radius of a droplet as a function of time, $a(t)$, was obtained by analysing the angular distribution of scattered light irradiance within the framework of the Mie theory (angle-resolved static light scattering). This is a well-established interferometric technique. Its variants (laser imaging for droplet sizing (ILIDS), interferometric particle imaging (IPI), Mie scattering imaging (MSI), interferometric Mie imaging (IMI), etc) are used for particle sizing e.g. in sprays (see e.g. [87] and references therein). The variant of this technique that we developed is outlined in [88] (experiments with water) and in [89] (experiments with slowly evaporating liquids). Green (532.07 nm) p-polarized and red (654.25 nm) s-polarized coaxial, counter propagating laser beams of ∼10 mW power each (inside the trap) and ∼0.5 mm waist were used simultaneously for droplet illumination. Droplet heating and direct momentum transfer from the beam could be neglected. The droplet was in the focal point of the objective lens (with a confocal filter). We recorded (up to ∼40 fps, 640 × 480 pixels, 12-bit, PixelFly colour camera, pco.imaging) out-of-focus images produced by the scattering of both beams (see top inset in figure 4). The field of view corresponded to 32.48 ± 0.02°. Its centre was at the azimuthal angle of 90 ± 0.1° and the elevation angle of 0 ± 0.3°. The field of view was horizontally divided into halves with perpendicular (s and p) polarizers. Having attributed different polarizations to different colours enabled the easy checking of polarizer

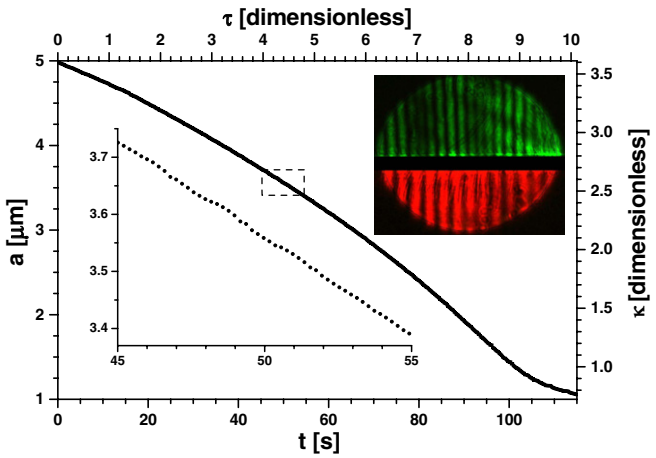

Figure 4. A typical evolution of the radius of a diethylene glycol droplet under standard temperature and pressure conditions. Dimensionless coordinates $\kappa = a/a_C$ and $\tau = t/t_C$ (see section 5), where the characteristic length scale $a_C = 1.38\,\mu$m and the characteristic time scale $t_C = 11.37$ s. The region at the end, after the 'kink', corresponds to the strong influence of impurities. Bottom inset: the magnification of the region bound with the dashed box. Top inset: an example of a Mie scattering image collected during this experiment.

leaks (proper setup) and monitoring of depolarization. In the case of homogeneous droplets, light depolarization was also used to indicate contamination with solid particles. The sequence of images was analysed off-line with our software (written in MATLAB). Each image was integrated with a proper distribution function over the elevation angle to ensure a better signal-to-noise ratio. The analysis was based on comparing the azimuthal distribution of irradiance observed in each image to the library of patterns obtained with the aid of Mie theory. Performing analysis for two polarizations simultaneously and for the whole $a(t)$ evolution rather than for separate points only, enabled to reduce some experimental uncertainties significantly. For instance, the position of interference fringes as a function of a depends on polarization, while misalignment of the objective versus laser beams introduces the same error to the azimuthal angle of observation for both polarizations. Such systematical errors can be easily accounted for in the optimization procedure. Similarly, 'defocusing' the imaging channel introduces systematic errors to the angular range of the field of view. This may cause significant errors in the readings of a but, fortunately, usually such error results in discontinuities in $a(t)$ and thus can be corrected by optimization as well. The latter procedure also allows us to overcome the difficulties in the interpretation of narrow resonances ($\leqslant$0.5 nm HWHM). Such resonances are very sensitive to many factors, like image integration over CCD exposition time or even slight droplet non-sphericity, which results in readings of a visibly off the trend. The average uncertainty of $a(t)$ for DEG was estimated from numerical experiments to be $\sim \pm 8$ nm (compare bottom inset in figure 4). For experiments with water it was by a factor of two larger. This error, although very small, is due to several factors, of which we would like to address the main ones. The uncertainty of the refractive index is the most important source of error among uncertainties of the parameters of the theory. For DEG, the manufacturer declared the refractive index with the accuracy of ± 0.001. This error in the index, on average corresponds to ± 3 nm uncertainty in $a(t)$. The maximal possible water content change of 0.03% corresponds (assuming rapid component mixing, see [89, 90]) to ± 0.1 nm uncertainty in $a(t)$. The total influence of the evaporation of volatile impurities (maximal content change of $<$0.3% (DEG)) corresponds to less than ± 1 nm uncertainty in $a(t)$. Larger systematic errors of the refractive index (e.g. in the case of unreliable compound lot data) can be detected and corrected with the procedures described above. The angular resolution of a recorded image was (depending on the setup implementation) $\sim \pm 0.02^\circ$. This error, on average, corresponds to ± 2 nm uncertainty in $a(t)$. Similar $a(t)$ uncertainty is associated with the uncertainty of the angular range of the field of view.

5. Theory versus experiment

Some insight into the range of applicability or the advantages of the different formulae encountered in the literature (i.e. (4), (6), (11) and (12)) describing evaporation of a droplet, can be gained from the analysis of the results of experiments on DEG and water of the IF PAN group [43, 89] and the MD numerical experiments of the IChF PAN group [25, 26].

Regardless of the details of the model it seems indispensable to account for kinetic effects. In this work we consistently use the effective diffusion coefficient (14) for the transport of mass and effective heat conductivity (15) for the transport of heat. As long as all the parameters can be regarded as constants (in particular $T_\mathrm{L} = \mathrm{const}$), equations (4), (6), (11) and (12) take the same general form of

$$\dot{a} = \frac{P_1}{a/(1 + P_3/a) + P_2}. \tag{19}$$

The kinetic effects are described with a single parameter $P_2 \sim 1/\alpha_{\mathrm{C,T}}$ and $P_3 = \Delta_\mathrm{C}, \Delta_\mathrm{T}$. It also follows, that the equations for the transport of mass can be treated separately from the equations for the transport of heat. Introducing the characteristic length and time scales κ and τ (compare remarks concerning formulae (14) and (15)) enables to express (19) in a dimensionless form:

$$\frac{\mathrm{d}\kappa}{\mathrm{d}\tau} = \frac{-1}{\kappa(1 + P_3/(\kappa P_2)) + 1}, \tag{20}$$

where $\kappa = a/P_2$ and $\tau = -tP_1/P_2^2$. Using the dimensionless form often greatly facilitates comparing different evolution cases (compare e.g. [91]).

It is worth noticing that the ratio P_3/a controls the form of the droplet evolution equation. Since $\Delta_\mathrm{C}, \Delta_\mathrm{T} \ll a$ for micrometre-sized droplets under STP conditions, P_3 can be rightfully neglected within experimental accuracy. This conclusion is upheld by the analysis of the MD simulations at the nanoscale presented further on. Thus, the considered equations take a very convenient form:

$$\dot{a} = \frac{P_1}{a + P_2}, \tag{21}$$

or an even simpler dimensionless form:

$$\left(\frac{\mathrm{d}\kappa}{\mathrm{d}\tau}\right)^{-1} = -(\kappa + 1). \tag{22}$$

Since the experimentally obtained $a(t)$ can be represented in $\dot{a}(a)$ form and P_1 and P_2 remain constant, (21) does not require integration. Since $(\dot{a})^{-1}$ is a linear function of a, P_1 and P_2 can be found with a linear fit. It seems to offer a convenient tool for the assessment of the model and measurement of the thermodynamic conditions/parameters. The drawback of this approach, which must be admitted here, is that the noise present in the experimental data gets magnified due to differentiation.

In figure 5 we present the evolution of the DEG droplet from figure 4, redrawn in $(\dot{a})^{-1}(a)$ form, while a representative example of water droplet radius evolution is shown in figure 6 in the same form. Both plots exhibit a region which is linear (within the limits set by the noise present in the data) and shifted versus the origin. It indicates that (21) applies and the kinetic effects must indeed be accounted for (with (14) or (15), respectively). The best fit for $P_2 = 0$ (no kinetic effects) is represented in figure 5 by a dashed line. On the other hand considering the HKL (2.1) only (purely kinetic-limited evaporation), as long as $T_\mathrm{L} = \mathrm{const}$ leads to $\dot{a} = \mathrm{const}$, which is obviously not the case. For the conditions corresponding to figure 5 $\alpha_\mathrm{C} = 0.08$, $1/\dot{a} \simeq -9\,\mathrm{s}\,\mu\mathrm{m}^{-1}$.

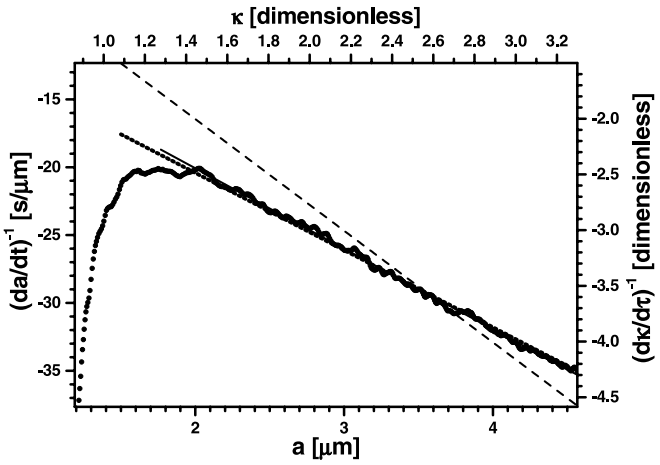

Figure 5. Evolution of the diethylene glycol droplet from figure 4 presented in $\dot{a}(a)$ form. Characteristic scales for the dimensionless coordinates: $a_C = 1.38\,\mu$m and $t_C = 11.37$ s. Strong undulations result from differentiation in data processing. The non-linear region for $a < 2\,\mu$m signifies the strong influence of impurities (see also figure 2). The dashed line corresponds to the best fit for $P_2 = 0$ (no kinetic effects), the dotted line to calculated P_1 and fitted P_2 and the solid line to both fitted P_1 and P_2.

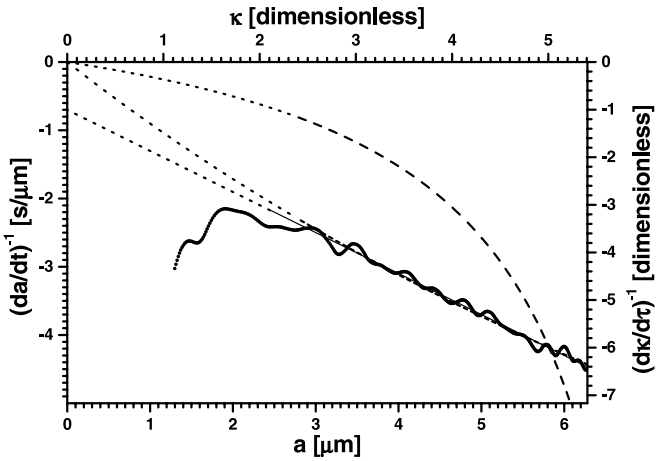

Figure 6. Water droplet radius evolution in $\dot{a}(a)$ form. Characteristic scales for dimensionless coordinates: $a_C = 1.16\,\mu$m and $t_C = 0.81$ s. Evaporation into (nearly) saturated water vapour/nitrogen atmosphere at 20 °C and 998 hPa. The non-linear region signifies the strong influence of impurities. The solid line represents a linear, two-parameter fit to the apparently linear region (21). Dashed and short-dashed lines correspond to two- and three-parameter SRT fits, respectively (section 5.4). All fits extended towards $a = 0$ with dotted lines.

5.1. Evaporation limited by diffusion of molecules in the vapour.

In view of the considerations from section 2.1, negligible Stefan flow (6) together with (14) may be written down as

$$\dot{a} = \frac{DM\,[p_\infty/T_\infty - p_a(T_L)/T_L]\,/(R\rho_L)}{a + D\sqrt{2\pi M/(RT_L)}/\alpha_C}. \qquad (23)$$

Then, comparing equations (23) with equation (21) we find

$$P_1 = DM\,[p_\infty/T_\infty - p_a(T_L)/T_L]\,/(R\rho_L),$$
$$P_2 = D\sqrt{2\pi M/(RT_L)}/\alpha_C. \qquad (24)$$

If quantities comprising P_1 (in particular D, p_∞, T_∞, T_L and $p_a(T_L)$) are known, only P_2 must be fitted, yielding α_C. However, in general $p_\infty/T_\infty - p_a(T_L)/T_L$ is a parameter analogous to $T_\infty - T_L$ in equations (11) and (12) (see also below). Fitting a single parameter P_2 is less vulnerable to the influence of impurities than fitting both parameters. Since the evaporation of a droplet is driven by the vapour density gradient, as can be easily seen from (23), $\dot{a}(a)$ is extremely sensitive to changes of vapour density, both at infinity and at the droplet surface. For instance, relative variations of p_∞ of the order of 0.1% induce noticeable effects, while 1% seems to be the limit of measurement accuracy in an atmosphere close to STP conditions. The issue of the accuracy of measuring the vapour density (vapour saturation, relative humidity) has been raised e.g. in [73] and [39]. As the inherent result of measurement techniques (for review see e.g [92]) partial vapour pressure is usually expressed in terms of the saturated vapour pressure. Apart from the intrinsic accuracy of empirical formulae for the saturated vapour pressure for many compounds, and in particular for water under STP conditions, the 0.1 K inaccuracy of vapour temperature measurement leads to ∼1% inaccuracy in the saturated vapour pressure. However, assuming that we know T_∞, T_L and $p_a(T_L)$ as well as other parameters with sufficient accuracy (which in many cases is possible), we can find $p_\infty/T_\infty - p_a(T_L)/T_L$ by fitting P_1 in the region free from influence of impurities and calculate p_∞. This constitutes a method of measuring the vapour pressure.

5.2. Evaporation limited by the transport of heat.

Similarly as for the transport of mass, (12) together with (15) for the transport of heat can be written as:

$$\dot{a} = \frac{-\lambda\,(T_\infty - T_L)\,/(q_{\rm eff}\rho_L)}{a + \lambda\sqrt{2\pi M_{\rm air}/(RT_L)}/(\alpha_T\rho c_P)}, \qquad (25)$$

which corresponds to

$$P_1 = -\lambda\,(T_\infty - T_L)\,/(q_{\rm eff}\rho_L),$$
$$P_2 = \lambda\sqrt{2\pi M_{\rm air}/(RT_L)}/(\alpha_T\rho c_P). \qquad (26)$$

In general, T_L is experimentally accessible with very limited precision (e.g. ±2 K in [44]). Even $T_L - T_\infty$ is not experimentally verifiable for the range of mK. On the other hand, if the model is correct, the procedures described above may serve finding $T_L - T_\infty$ with high accuracy and thus finding T_L with accuracy limited only by the accuracy of T_∞. Further on, (25) should hold also when $T_L(t)$ is a function of time ($P_1 \neq$ const). This is applicable in the presence of impurities, as long as they do not modify the major parameters. Thus, it is possible to follow the evolution of T_L some way into the impurity-controlled region of droplet evolution.

Still, it must be kept in mind that T_L is easily and accurately accessible in MD simulations (shown in section 6).

5.3. Slower versus faster evaporation

For the conditions of our experiments, for both slower and faster evaporation, $T_L \simeq T_\infty$ can be expected. Thus, $T_L = T_\infty$

can be used in equations (4), (6) and (7) as well as in (14) and (15), though under no circumstances in (11) and (12). Furthermore, since the droplets were micrometre-sized, the influence of surface tension was negligible and $p_a(T_L) = p_{sat}(T_L) = p_{sat}(T_\infty)$.

Slower evaporation. We shall address the results of the experiments on slowly evaporating liquids first, since their description is relatively simple. Here, the experimental conditions and procedures allow us to additionally set $p_\infty = 0$ and $q_{eff} = q$. As it has been mentioned in section 2, the results for DEG droplets correspond to $Le \gg 1$, so the equations describing the transport of mass cannot be automatically interchanged with equations describing the transport of heat.

The dotted line in figure 5 corresponds to a one-parameter (P_2) fit of (21) to the apparently linear part of the plot, with P_1 calculated from literature data [93, 94] and formula (24). It yielded $\alpha_C = 0.075$. On the other hand, for the solid line in figure 5, P_1 was fitted together with P_2. It yielded a value higher than calculated by ~4%. It seems to indicate (in view of section 3.1) that the residual uncertainty of the input data and parameters was higher than the possible effect of impurities. Such a result is quite satisfactory and indicates that after gathering sufficient statistics a reliable value of α_C could be found.

In the case of heat transport equations, a similar twofold approach is possible:

(i) We can calculate P_1 from formula (24), insert it into (26), calculate T_L, fit P_2 only (the dotted line in figure 5) and find α_T. We expect that the value of T_L, obtained in this way, corresponds to ideal conditions when no impurities or other similarly acting factors are present. This also seems a better way for finding α_T for a pure liquid. For the case presented in figure 5 we found $T_L - T_\infty = 4.1$ mK and $\alpha_T = 0.12$.

(ii) We directly fit P_1 and P_2 (the solid line in figure 5) and find T_L and α_T from (26). This would correspond to real T_L and α_T for a real, actual liquid. In this way we found $T_L - T_\infty = 4$ mK and $\alpha_T = 0.13$.

Faster evaporation. The evaporation of water droplets ($Le \simeq 1.16$) is essentially faster than the evaporation of droplets of DEG. However, since the droplet evaporates into a highly humid atmosphere, p_∞ is significant. There remains an open question whether we can still set $q_{eff} = q$, which we do for the lack of better data. Since q_{eff} divides the experimentally unknown $T_\infty - T_L$ we cannot resolve this problem here.

Applying formula (26) to data presented in figure 6 (solid line) yielded $T_\infty - T_L = 0.15$ K and $\alpha_T = 0.15$, while with formula (24) (the same solid line) we found $\alpha_C = 0.14$ and $S = 0.996$, where S is saturation or, in the case of water vapour, relative humidity, $p_\infty = S p_{sat}(T_\infty)$. Such a value of S is in perfect agreement with our experimental technique. If p_∞ is very close to $p_{sat}(T_\infty)$ and/or the droplet radius is very small, the Kelvin relation (5) may also have to be utilized, but then $1/\dot{a}(a)$ becomes non-linear and (21) would fail. In such a case a complete set of equations (6), (12), (14), (15) together with (5) (as in section 3.1) and a multi-parameter fit, as described in [43], must be used. In order to verify our results, though we did not enter such a non-linear region, we performed the multi-parameter fit. The results are in excellent agreement with those from the analysis presented above, except for α_T which was found to be close to 1. Since α_T is a second order parameter in the multi-parameter fitting of the equation set, the method presented above seems to be more reliable. However, as it has been mentioned, most authors obtained values close to unity.

5.4. Statistical rate theory

Another way to tackle the problem of evaporation has been consequently proposed by Ward *et al* (see e.g. [23, 36, 95]). They applied SRT to non-equilibrium evaporation in a single-component system. The evaporation probability of a molecule is introduced and initially considered quantum-mechanically, though quantum-mechanical calculations are circumvented by introduction of the Boltzmann definition of entropy and the kinetic theory description of equilibrium. It must be pointed out that the equilibrium evaporation probability of a molecule was assumed to be unity: $\alpha_C = 1$. We shall discuss this issue later on in view of the experiments of Davidovits, performed under the equilibrium conditions with isotopically labelled molecules [55]. In the case of a droplet of water, the resulting SRT formulae take the form:

$$\dot{a} = -\frac{2\eta}{\rho_L(T_L^i)} \frac{p_{sat}(T_L^i)}{\sqrt{2\pi k T_L^i}} \sqrt{m} \sinh\left(\frac{\Delta s^{LV}}{k}\right), \tag{27}$$

where

$$\eta = \exp\left[\frac{m}{\rho_L(T_L^i) k T_L^i}\left(P_L^e - P_{sat}(T_L^i)\right)\right], \tag{28}$$

$$\begin{aligned}\frac{\Delta s^{LV}}{k} = {} & \ln\left[\left(\frac{T_V^i}{T_L^i}\right)^4 \frac{P_{sat}(T_L^i)}{P_V^i}\right] + \ln\left[\frac{q_{vib}(T_V^i)}{q_{vib}(T_L^i)}\right] \\ & + 4\left(1 - \frac{T_V^i}{T_L^i}\right) + \left(\frac{1}{T_V^i} - \frac{1}{T_L^i}\right) \\ & \times \sum_{l=1}^{3n-6}\left[\Theta_l/2 + \frac{\Theta_l}{\exp(\Theta_l/T_V^i) - 1}\right] \\ & + \frac{m}{\rho_L(T_L^i) k T_L^i}\left(P_V^i + \frac{2\gamma}{a} - P_{sat}(T_L^i)\right),\end{aligned} \tag{29}$$

$$q_{vib}(T) = \prod_{l=1}^{3} \frac{\exp\left[-\Theta_l/(2T)\right]}{1 - \exp\left(-\Theta_l/T\right)} \tag{30}$$

and P_L^e must satisfy

$$P_L^e - \frac{2\gamma}{a} = \eta P_{sat}(T_L^i). \tag{31}$$

T_L^i and T_V^i are the interfacial liquid and vapour temperatures, P_V^i is the pressure in the gas at the interface, P_L^e is the liquid pressure at equilibrium, n is the number of atoms in the evaporating molecule and Θ_l is the molecular vibrational temperature.

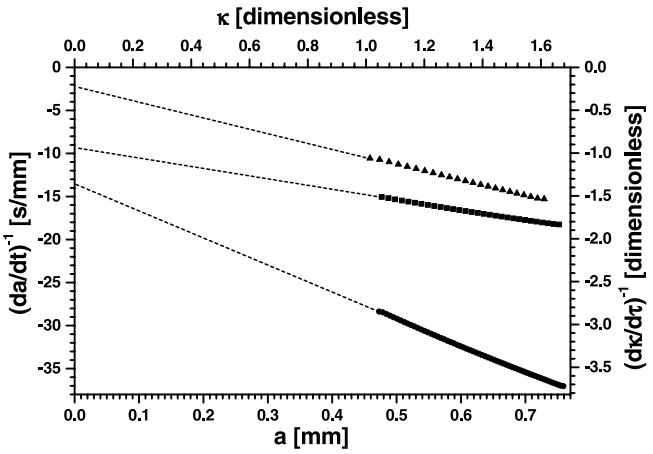

Figure 7. The evaporation of water droplets into water vapour, from [36], presented in $1/\dot{a}(a)$ form. Characteristic scales for dimensionless coordinates: $a_C = 453\,\mu$m and $t_C = 4500$ s, taken as averages over the presented data sets. All these experimental data seem to conform to (21) with non-zero P_2: linear extrapolations towards $a = 0$, shown as dotted lines, are not pointing towards (0,0), while SRT predicts otherwise.

The applicability of SRT to the evaporation of an argon droplet into its own vapour will be discussed in section 6. By definition, application of this model to the evaporation of a water droplet into standard air or nitrogen may require some adaptations. Here we tried to apply this model as it stands. However, apart from fundamental issues, in the case of our experiments with levitated droplets neither T_L^i, T_V^i nor P_V^i were accessible. However, for higher pressures (compare [28, 36]), the temperature discontinuity at the interface is expected to be negligible and we assumed $T_L^i = T_V^i$. Apart from that, we assumed $P_V^i = p_\infty = Sp_{sat}(T_\infty)$. Fitting the above model to the data presented in figure 6 yielded $T_L^i = 292.66$ K and $S = 0.97$, which are in reasonable agreement with the results presented in section 5.3 ($T_L^i = 292.96$ K, $S = 0.996$ and $\alpha_C = 0.19$), though the functional dependence presented in figure 6 (dashed line) seems totally wrong. This can be partially improved by introducing α_C as a third fitting parameter. Then we obtain $T_L^i = 292.92$ K, $S = 0.990$ and $\alpha_C = 0.19$ which are in excellent agreement with our results and the functional dependence is reproduced better (the short-dashed line in figure 6). However, the model predicts non-linear $1/\dot{a}(a) \to 0$ for $a \to 0$ which was illustrated in figure 6 for both sets of optimized parameters, while the results of our experiments suggest otherwise. Furthermore, the results of Ward *et al* in the $1/\dot{a}(a)$ representation (see figure 7) appear also to be linear and do not point towards (0,0). The model is nearly linear in a form of $1/\dot{a} \propto a$ when the term $\Delta s^{LV}/k$ (linked to the entropy change associated with the molecular transition through the interface; formula (30)) is small. This happens when e.g. the temperature at the interface is nearly continuous. However, (27), representing the model, never takes the form of (21). It indicates that additional factors (perhaps just the presence of impurities) should be considered. Since the functional dependence of [36] data coincides with equations (21) and (19), we may find the predictions of Maxwellian theory with a kinetic extension. We shall start with (21) as evidently reproducing the data. In the case of evaporation into vapour, there is no Stefan flow and in the case of (21), formulae (24) and (26) can be used. We calculated the self-diffusion coefficient with equation (18) of [36], taking the temperature of the reservoir as the reference temperature: $T_{ref} = T_\infty$. We calculated the thermal conductivity of water vapour with the equation given in [96] for the same temperature. We considered test 2 of [36] (initial pressure: 2880 Pa, reservoir temperature $T^B = 300.02$ K and $T^B - T_i^L \simeq 3$ K) and found $T_\infty - T_L = 4.3$ K and $\alpha_T = 0.007$. Then, using T_L, we obtained $p_\infty = 2770$ Pa. While the values of $T_\infty - T_L$ and p_∞ are reasonable, α_T seems much too low. Since, under the considered thermodynamic conditions the mean free path is relatively long, it may be expected that (19) should be used instead of (21). However, the smallest χ^2 is obtained for $P_3 = 0$. Thus, we conclude, that the droplet was much too large for kinetic effects to manifest in the Maxwellian model and a reliable value of α_T could not be found.

6. Molecular dynamics simulations

The models discussed in the previous sections have been derived on the basis of a continuous description of fluids with kinetic corrections to describe the evaporation of micrometre-sized droplets. In this section we examine these models by comparing their results with those of the computer simulation of the evaporation of nanodroplets. The simulation, where we only assume a form of intermolecular potential, is a good tool to model droplet evaporation because all conditions of the simulated process are controlled and all quantities that characterize the process can be determined independently. The simulation should be performed under conditions as close as possible to those occurring in experiments. However the number of molecules in a computer simulation is many orders of magnitude smaller than the number in an experiment. Therefore a number of conditions have to be satisfied before we can compare the physical results of computer simulations to those from experiments. Some minimum requirements are listed below:

(i) In a typical experiment the droplet is immersed in a finite container. The boundaries are kept at constant temperature T_∞. The distance from the droplet centre to the boundary R_∞ is very large in comparison to the nanoscale study of computer simulations. We assume that far from the droplet surface the gas parameters do not change during the evaporation process. In the computer simulation R_∞ cannot be so large, however it is possible to get the number of molecules large enough to fulfil this condition approximately. Landry *et al* [40] proposed the method in which the gas parameters are kept constant by removing the gas molecules. Even in such a case R_∞ cannot be low, since the distance from the droplet surface to the boundaries divided by the mean free path, $n_{rat} = (R_\infty - a)/l_a$, should be large enough to assure that heating the gas at the boundary does not influence the evaporation process directly.

(ii) In a typical experiment the droplet radius is equal to a few micrometres. As a result, the influence of the width of the interface on time evolution is very low. The resulting minimum requirement for the simulation is that the droplet radius should be much larger than the width of the interface. Considering the values of the surface width parameter for the Lennard-Jones (LJ) liquid [97], we can assume that a should not be significantly lower than 10σ where σ is the LJ length parameter.

(iii) In experiment a/R_∞ can be set to 0, while this value is finite in computer simulations. Therefore we have to account for the finite size of the system in any comparison with experiment.

The above conditions ((i) and (ii)) are fulfilled only if the total number of molecules N in the simulation is large. Most simulations that can be found in the literature concern the evaporation of very small LJ droplets [40, 98, 99]. The results were very interesting but N, not higher than a few thousand, was much too low to fulfil both (i) and (ii). Walther and Koumoutsakos [41] (WK) performed simulations where N was an order of magnitude larger. They modelled the evaporation of the LJ atom droplet at supercritical conditions and concluded that the temporal evolution of droplet radius $a(t)$ obeys the classical 'D^2 evaporation law' (as (7) or (12)):

$$\frac{\mathrm{d}a^2}{\mathrm{d}t} = \text{const.} \tag{32}$$

They used formula (11) under the condition of $Le = 1$ to fit their data. The number of LJ atoms in the droplet applied by WK was enough to satisfy the condition (ii). The simulation box was also large, but n_{rat} amounted only to about 2, which seems to be too low.

Hołyst and Litniewski [25] (HL) have presented the results of large scale (N over 2.6×10^6) computer simulations of evaporation of the LJ liquid droplet surrounded by the vapour, all enclosed in a spherical vessel of radius $R_\infty \gg l_a$. The boundaries were kept at the constant temperature $T_\infty > T_\mathrm{c}$ where T_c was the critical temperature. The evaporation was simulated for different conditions with $T_\mathrm{L}/T_\mathrm{c}$ varying from 0.678 to 0.955. The total number of LJ atoms was large enough to satisfy both (i) and (ii). R_∞/a was always larger than 7 and n_{rat} was never lower than 10. HL have also proposed how to take into account the finite size of the gas container (condition 3). In a typical experiment the heat is transferred from R_∞ to the droplet surface and R_∞ is so large that a/R_∞ can be assumed to be 0. In computer simulations R_∞ is not so large and its value influences the obtained results. The influence can be taken into account as in the hydrodynamic model [28, 32] in which the result of the integration of the heat transport equation (HTE), as e.g. (8), depends on the boundaries: both on a and on R_∞. Simplifying HTE [28], the 'D^2 law' ((32)) is fulfilled only if $a/R_\infty \to 0$. On the other hand, (32) is fulfilled for all $R_\infty > a$ if we replace a with [25]:

$$a^* = a\left(1 - \frac{2a}{3R_\infty}\right)^{1/2}. \tag{33}$$

This result strongly suggests that if a/R_∞ cannot be neglected, the time evolution of the droplet radius of an experimental system is better described by $a^*(t)$ than $a(t)$. In this way we satisfy condition (iii) which is necessary to compare the results of experiments to those of computer simulations.

In the following, we use the computer simulation data from the HL work (listed in table I in [25]) to test the theoretical formulae for $\mathrm{d}a^*/\mathrm{d}t$. In the simulations, a was defined as the distance from the droplet mass centre to the point where the density is equal to half of the mean density of the droplet. All the results given below are expressed in units of argon assuming the mass $m = 40$ a.m.u. and the LJ parameters: $\sigma = 3.4\times10^{-10}$ m, $\varepsilon = 140.5k = 1.939\times10^{-21}$ J. The temperature scale is obtained by adopting the critical temperature for the LJ potential truncated at $r_\mathrm{c} = 2.5\sigma$ ($T_\mathrm{c} = 1.08$ in the reduced units [97]) equal to the temperature for argon (151.75 K).

Using the computer simulation data of HL [25] we estimated the gas density just above the droplet surface ρ_a. We determined the diffusion coefficient in the vapour D and the heat capacity c_p for the gas density ρ_a by performing additional short computer simulations on the 125 000 particle systems using the constant energy and volume molecular dynamics (MD) method [100]. The values of D at ρ_a, further denoted as D_a, were determined using the Einstein formula [100] for all values of liquid temperature considered here. The specific heat has been estimated for two state points: $c_p = 2.8R$ for $\rho/m = 0.165\,\mathrm{nm}^{-3}$, $T = 102.7$ K and $c_p = 3.7R$ for $\rho/m = 0.832\,\mathrm{nm}^{-3}$, $T = 128.1$ K. The values of c_p together with λ from the supplementary information to the HL paper [25] gives $Le = 1.06$ and 0.92, respectively, which shows that in our case, the assumption $Le \approx 1$ is a reasonable approximation.

First, an important result that we have found analysing the simulation data is that the time evolution of the inverse of $\mathrm{d}a^*/\mathrm{d}t$ in a quasi-stationary regime (the second part of the time evolution) is a strictly linear function of a^* (formula (21)). We fitted $(\mathrm{d}a^*/\mathrm{d}t)^{-1}$ with the function $f_{\mathrm{fit}}(a^*)$ being the inverse of the general formula (19):

$$\left(\frac{\mathrm{d}a^*}{\mathrm{d}t}\right)^{-1} = f_{\mathrm{fit}}(a^*) = -\frac{1}{P_1}\left(\frac{a^*}{1+P_3/a^*} + P_2\right), \tag{34}$$

where now P_1, P_2 and $P_3 \geqslant 0$ are adjustable constants. The curves resulted from the minimization for selected data are shown in figure 8 ($(\mathrm{d}a^*/\mathrm{d}t)^{-1}$ versus a^*). Initially (large a^* in figure 8) the system was heated at the boundary and a sudden change of temperature resulted in sound waves travelling in the system. For this time period (34) was not valid. For the rest of the time, the evaporation process was well described by the linear dependence of $(\mathrm{d}a^*/\mathrm{d}t)^{-1}$ versus a^* (figure 8). According to (33) $\mathrm{d}a^*/\mathrm{d}t = (\mathrm{d}a/\mathrm{d}t)[1 - 2a/(3R_\infty) + O(a^2/R_\infty^2)]$. The differences in the quality of the fit (determined by χ^2) for $(\mathrm{d}a/\mathrm{d}t)^{-1}$ and $(\mathrm{d}a^*/\mathrm{d}t)^{-1}$ were non-significant. The only, physically important, difference was that the values of P_1 for a^* were higher than that for a by 13 to 20% of the relative value. The presence of P_3 in (34) did not improve the quality of the fit. For the temperature of the liquid droplet $T_\mathrm{L} < 122$ K the minimization always gave $P_3 = 0$. For larger T_L, P_3 was usually non-zero but the difference between the corresponding χ^2 and that for $P_3 = 0$ was always non-significant. Following the discussion on the meaning of Δ_C

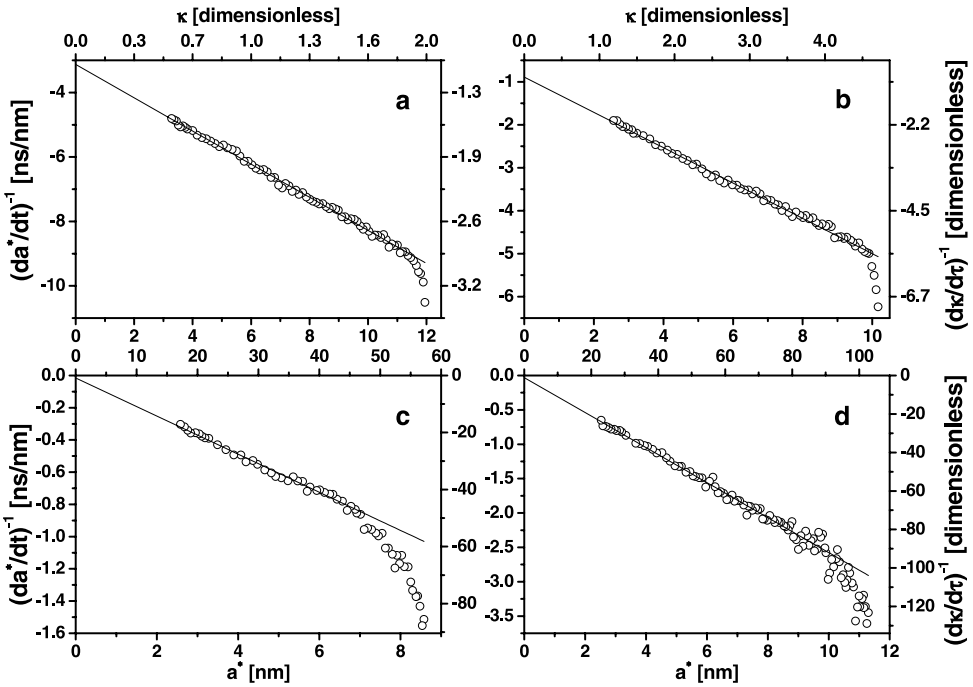

Figure 8. The inverse of $\mathrm{d}a^*/\mathrm{d}t$ versus a^*. The empty circles give the minimization data obtained by numerical differentiation of $a^*(t)$ from the simulation. The solid line gives $f_{\mathrm{fit}}(a^*)$ from the minimization of P_1 and P_2 for $P_3 = 0$ in (34). Figures (*a*), (*b*), (*c*) and (*d*) give the results for the simulations for $n_0 = 1$, 3, 6 and 8 (table 1), respectively. The characteristic scales for dimensionless coordinates are: (*a*) $a_{\mathrm{C}} = 6.1$ nm, $t_{\mathrm{C}} = 19.1$ ns; (*b*) $a_{\mathrm{C}} = 2.16$ nm, $t_{\mathrm{C}} = 1.92$ ns; (*c*) $a_{\mathrm{C}} = 0.15$ nm, $t_{\mathrm{C}} = 2.7$ ps; (d) $a_{\mathrm{C}} = 0.11$ nm, $t_{\mathrm{C}} = 3.1$ ps. In the case of (*a*) the mean free path in the gas phase is comparable to the radius of the droplet (see $n_0 = 1$ in table 1). The highly non-linear data for high a^* ($a > a_{\max}$ (see table 1)) correspond to the initial transient non-stationary regime related to travelling sound waves [25] and are not taken into account in the minimization.

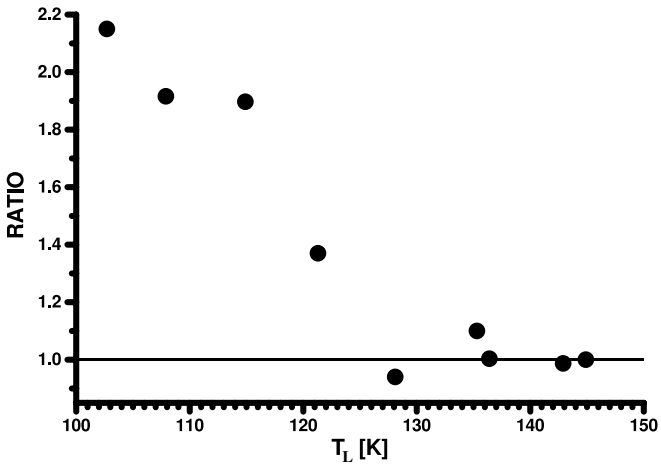

Figure 9. The ratio (RATIO; solid dots) of χ^2 from the fit (see (34)) for $P_3 = l_a$ to χ^2 for $P_3 = 0$ versus T_{L} for the simulations from table 1. The horizontal line corresponds to RATIO = 1. The quality of the fit with (34) is the best for $P_3 = 0$; for any non-zero P_3 the quality of the fit deteriorates. Therefore, not only in experiment but also at the nanoscale, this parameter can be neglected in (19) and (34).

(see (14)) we compared the minimization results for $P_3 = 0$ and $P_3 = l_a$. The ratio of χ^2 for $P_3 = l_a$ to χ^2 for $P_3 = 0$ versus T_{L} is given in figure 9. From this analysis we see that non-zero P_3 makes the quality of the fit worse.

The values of P_1 and P_2 are presented in table 1. Table 1 comprises also the maximum $a_{\max}$ and the minimum $a_{\min}$ values of a for which the fits were done, the mean free path l_a and the diffusion constant D_a for the gas at the liquid temperature T_{L} and the density ρ_a just above the droplet surface. The mean free path was estimated from [101]:

$$l_a = \left(\pi\sqrt{2}\sigma^2\rho_a\right)^{-1}. \tag{35}$$

The simulation of HL [25] allows us to test the theoretical models discussed in the previous section. First we compare the values of P_1 obtained from (34) with the theoretical value from (12). In the theoretical formulae we assumed T_{L} as time independent. This is only an approximation. In analysing the simulation data we found that the droplet temperature slightly decreased when a became lower than about 3.5 nm. The temperature decrease at $a = a_{\min}$ never exceeded 3% of the relative value of the temperature change. The values of $a_{\min}$ and $a_{\max}$ from table 1 clearly show that the error associated with the assumption of $T_{\mathrm{L}} = \mathrm{const}$ is negligible.

Hołyst and Litniewski simulated a one-component system, so the theoretical prediction of P_1 reads, according to (12) and (26), as

$$P_1^{\mathrm{pred}} = -\frac{\lambda\,(T_\infty - T_{\mathrm{L}})}{\rho_{\mathrm{L}} q_{\mathrm{eff}}}. \tag{36}$$

Table 2 shows P_1 and P_1^{pred}. The relative error $\delta P_1 = P_1^{\mathrm{pred}}/P_1$. The approximation for P_1 appears to be very reasonable. $|\delta P_1|$ exceeds 0.1 only if both T_{L} and $(T_\infty - T_{\mathrm{L}})$ are high. We found also that the absolute values of the prediction errors are significantly lower for a^* than for a, which confirms that if we compare computer simulations with experiment, the droplet radius should be redefined with (33).

Table 1. The computer simulation data, the minimization results and the parameters for the simulations from [25]. The sequence numbers n_0 correspond to those from table 1 of [25]. P_1 and P_2 (see equations (21) and (19)) are obtained from the minimization of $f_{\rm fit}(a^*)$ (formula (34)) for $P_3 = 0$. ρ_a is the density of gas close to the droplet surface and D_a is the diffusion coefficient obtained from the simulation at ρ_a and $T_{\rm L}$. $T_{\rm L}$ is the liquid droplet temperature during evaporation (almost constant as explained in the body of the text) and $\rho_{\rm L}$ is the liquid mass density. T_∞ is the temperature at the boundary of the container. $a_{\rm min}$ and $a_{\rm max}$ give the minimum and maximum values of the droplet radius a used during the minimization (see also figure 8) and l_a is the mean free path in the gas phase evaluated from (35).

n_0	$T_{\rm L}$ (K)	T_∞ (K)	$\rho_{\rm L}/m$ (nm^{-3})	ρ_a/m (nm^{-3})	D_a (mm^2 s^{-1})	P_2 (nm)	P_1 (nm^2 ns^{-1})	l_a (nm)	$a_{\rm min}$ (nm)	$a_{\rm max}$ (nm)
1	102.7	175.6	19.7	0.216	0.726	6.10	1.95	9.00	3.2	11.4
2	107.9	175.6	19.2	0.318	0.517	3.41	2.07	6.12	2.4	11.0
3	114.6	175.6	18.5	0.496	0.349	2.16	2.43	3.92	2.5	10.3
4	121.3	175.6	17.7	0.725	0.252	1.03	2.67	2.69	2.1	7.7
5	128.1	175.6	16.8	1.119	0.174	0.21	2.98	1.74	2.3	7.9
6	135.3	245.9	15.8	1.399	0.145	0.15	8.46	1.39	2.6	7.3
7	142.9	351.3	14.4	1.743	0.123	−0.03	16.90	1.12	2.4	8.0
8	136.4	175.6	15.6	1.705	0.122	0.11	3.93	1.14	2.5	10.2
9	144.9	245.9	13.8	2.099	0.104	0.01	13.12	0.93	3.4	9.7

Table 2. The comparison of P_1 from the minimization with $f_{\rm fit}(a^*)$ (see table 1) and the theoretical value of P_1 ($P_1^{\rm pred}$ from formula (36)). The approximation for P_1 appears to be very reasonable. The relative error in $P_1^{\rm pred}$ exceeds 0.1 only if both $T_{\rm L}$ and $T_\infty - T_{\rm L}$ are high.

n_0	$T_{\rm L}$ (K)	$T_\infty - T_{\rm L}$ (K)	P_1 (nm^2 ns^{-1})	$P_1^{\rm pred}$ (nm^2 ns^{-1})
1	102.7	72.9	1.95	2.09
2	107.9	67.7	2.07	2.21
3	114.6	61.0	2.43	2.45
4	121.3	54.4	2.67	2.72
5	128.1	47.5	2.98	3.05
6	135.3	110.6	8.46	8.24
7	142.9	208.4	16.90	19.29
8	136.4	39.2	3.93	3.54
9	144.9	101.0	13.12	12.01

As it has been already mentioned, SRT predicts $\dot{a}$ in a form different from (19). Table 3 compares $\dot{a}$ from the MD simulation with that predicted by SRT for $a = 20\sigma = 6.8$ nm. SRT predicts a non-physical result: $\dot{a}_{\rm SRT}$ is positive i.e. the droplet grows in time instead of decreasing its size. For the conditions given in table 3, p_V is significantly higher than $p_{\rm sat}(T_{\rm L})$. The first term in formula (30) becomes strongly negative and $\Delta s^{\rm LV}/k$ changes sign. It may be confirmed by an observation that significantly better results are obtained by setting up false $p_V = p_{\rm sat}(T_{\rm L})$. Then, the prediction given by $\dot{a}_{\rm SRTEQ}$ is not so poor if only $T_{\rm L}$ is low enough. SRT seems to gain accuracy for moderately non-equilibrium processes (see $T_\infty - T_{\rm L}$ in table 2).

We are not aware of any theory that predicts the value of P_2 successfully in the whole range of temperatures and densities. Assuming $Le \approx$ const, (26) predicts P_2 proportional to $D_a T^{-1/2}$. Taking into account (35), the assumption that P_2 is proportional to l_a/a [25] gives a very similar relation since $\rho_a D_a T^{-1/2}$ is a very weakly changing quantity (see table 1). In fact, the dependence of P_2 on thermodynamic variables is more complex. Assuming $Le = 1$, (26) gives, the following relation between $\alpha_{\rm T}$ and P_2:

$$\alpha_{\rm T} = \frac{D_a}{P_2}\sqrt{2\pi M/(RT_{\rm L})}. \tag{37}$$

According to figure 9, $\alpha_{\rm T}$ calculated from formula (37) as a function of ρ_a splits into two regions, those of high and low values. An important result that we have found when analysing the simulation data is that the jump in $\alpha_{\rm T}^{-1}$, which is seen in figure 10, is strictly correlated with the temperature discontinuity at the droplet surface that is shown in the HL paper [25]. The effect is evident if we compare the two panels of figure 10. Therefore we conclude that the high value of $\alpha_{\rm T}^{-1}$ found in experiments is a sign that kinetic effects are important and that their origin is in the temperature discontinuity measured for the first time by. Ward and his group [13]. For the continuous profile of the temperature across the interface $P_2 = 0$ and consequently $\alpha_{\rm T}^{-1} = 0$.

7. Summary

The temporal evolution of the radius of evaporating droplets follows (21), irrespective of whether it pertains to a single component (evaporation of the liquid into its own vapour) or multi-component system (evaporation of a liquid into a gas or vapour of another substance). This equation has two parameters: P_1 and P_2. P_1 is well described by the continuous irreversible thermodynamics approach in the form of formulae (24) or (26). P_2 is a correction arising from the kinetic theory of gases (again, see formulae (24) and (26)). The form of P_2 involves unknown evaporation coefficients. In the case of an evaporation of a liquid into its own vapour, P_2 is non-zero only if there is a temperature discontinuity at the interface.

The temperature discontinuity appears always for a sufficiently small density of the vapour phase. This fact indicates that the temperature jump at the interface is due to the momentum/pressure equilibrium. The explanation is very simple: for diluted vapour the pressure is given by the product of the vapour density and temperature. If the density is too low, only sufficiently high temperatures would guarantee momentum/pressure equilibrium. Thus equilibration of pressures (including the curvature term in the Laplace law for droplets) during evaporation is the main mechanism for the temperature discontinuity at the liquid–vapour interface.

Table 3. The comparison of $\dot{a}$ for $a = 6.8$ nm from the HL simulation (index $_{\text{sim}}$) with the value from the SRT model for p_V from the MD simulation and for the assumption of $p_V = p_{\text{sat}}(T_{\text{L}})$ (indices $_{\text{SRT}}$ and $_{\text{SRTEQ}}$, respectively). The surface tension γ and the saturation pressure $p_{\text{sat}}(T_{\text{L}})$ are taken from [97].

n_0	T_{L} (K)	γ (mJ m^{-2})	$p_{\text{sat}}(T_{\text{L}})$ (MPa)	p_V (MPa)	$\dot{a}_{\text{sim}}$ (nm ns^{-1})	$\dot{a}_{\text{SRT}}$ (nm ns^{-1})	$\dot{a}_{\text{SRTEQ}}$ (nm ns^{-1})
1	102.7	8.26	0.340	0.414	−0.151	0.168	−0.134
2	107.9	7.10	0.502	0.597	−0.203	0.220	−0.164
3	114.7	5.68	0.789	0.893	−0.271	0.222	−0.201
4	121.3	4.26	1.171	1.327	−0.341	0.406	−0.221
5	128.1	2.96	1.693	1.840	−0.425	0.374	−0.223
6	135.3	1.84	2.389	2.664	−1.218	0.898	−0.203
7	142.9	0.83	3.315	3.774	−2.495	1.710	−0.141
8	136.4	1.55	2.514	2.649	−0.568	0.378	−0.183
9	144.9	0.64	3.588	3.897	−1.927	1.172	−0.123

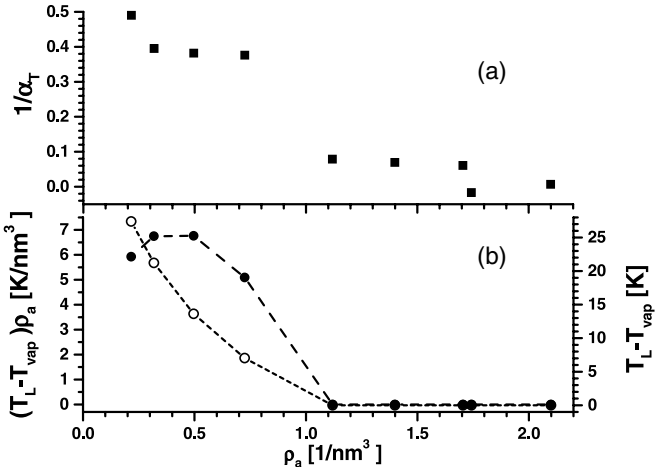

Figure 10. (*a*) The inverse of α_{T} constant calculated from (37) as a function of the gas density above the interface, ρ_a. The vales of P_2 are taken from table 1. α_{T} parameter is usually assumed constant in experimental studies. Here we show that its value depends on the gas density and therefore can vary from system to system depending on the thermodynamic parameters of the vapour phase. For a large vapour density this parameter becomes infinitely large which means that the concept of kinetic-limited transport (the ballistic motion of molecules) is not adequate. For lower values of ρ_a, the value of α_{T} is much more reasonable however the parameter cannot be simply interpreted as the probability [45]. Moreover the change of α_{T} is correlated with the discontinuity of temperature at the interface. For $\alpha_{\text{T}}^{-1} \approx 0$ the temperature is continuous at the interface (see figure 10). As α_{T} is related to the kinetic-limited transport we conclude that such transport significantly affects evaporation only for a low gas density correlated with temperature discontinuity at the interface. Such behaviour is characteristic for most experimental cases as discussed in the experimental section and as shown in the experiments of Ward [13, 36]. (*b*) Open circles: the difference between the liquid temperature T_{L} and the gas temperature at the interface T_{vap} (temperature jump at the interface, see [25]) as a function of the vapour density ρ_a. Solid dots: the temperature jump at the interface is inversely proportional to the density of the vapour phase (below some characteristic density in the system as shown in the figure). For a sufficiently high vapour density the temperature is continuous at the interface i.e. $T_{\text{L}} = T_{\text{vap}}$.

The evaporation is in the first place driven by the heat flux from the vapour phase. However lowering the vapour density would finally lead to the evaporation scenario being completely dominated by kinetic effects (not fully accounted for by formulae (26), where the kinetic term is only the correction to the main part). An extreme case is evaporation into vacuum, when the momentum flux density is equal to the liquid pressure and governs in this way the mass flux [26, 27]. In the latter case there is no heat flux from outside and during evaporation the droplet lowers its temperature.

For multi-component systems the situation is different and the scenario of evaporation changes, despite the fact that the same (21) is valid as in the single-component system. First of all the vapour has high density and momentum/pressure equilibrium is satisfied easily e.g. for water evaporating into the air. Therefore momentum/pressure equilibrium is not the constraint which governs density and temperature profiles as in the single-component system. We believe that the scenario of evaporation is as follows: the droplet is originally at the same temperature as the vapour/ambient atmosphere. After a short time the droplet lowers in temperature because of evaporation until the heat flux from the surrounding gas matches the enthalpy of evaporation. The temperature difference between the gas and the droplet is usually small and most probably the temperature is simply discontinuous at the interface. The temperature difference between the vapour and the droplet is defined by the evaporation mass flux and enthalpy of evaporation. The mass flux is most probably given by (13) once again with an unknown evaporation coefficient α_{C}.

It is feasible to find a reliable value of α_{C} (if necessary corrected for a higher droplet temperature drop). The results we obtained for water versus temperature are in excellent agreement with those obtained with a fundamentally different method of the BC/ARI group. The value of α_{T} is significantly lower than obtained with a multi-parameter fit and by most authors. Therefore we conclude that the problem of the evaporation coefficient is still open especially because there is no consistent theory which would explain its origin. The evaporation coefficients should be explained on the basis of equilibrium simulations of liquids in contact with their vapours. The experiments of Davidovits (see e.g. [66]) show that α_{C} is smaller than 1. It is not a surprise because the flux leaving the liquid surface is matched by a flux which reaches the surface of the liquid and is not reflected. If we take a classical Hertz–Knudsen equation for the mass flux, it should be multiplied by a factor which cuts out the flux that is reflected at the interface.

The experiments yield a number of specific conclusions: Accounting for kinetic effects is indispensable for droplets of

the radius $a < 5\,\mu$m evaporating into a standard atmosphere, regardless of the evaporation rate. Neither a diffusion only, nor kinetic only approach is successful. As long as $1/\dot{a}(a)$ is linear, it is sufficient to use the transport equations as given by (21). Δ_C and Δ_T can be neglected. Such a method is simple and quick. Accounting for the effects of temperature change with time turned out to be not necessary even for relatively fast evaporating droplets. The effect of surface tension is substantial only for the droplets evaporating into their own nearly saturated vapour. In dealing with pure liquids, the effects of impurities can be avoided by careful handling during experiment and using the strictly linear region of $1/\dot{a}(a)$ data during data processing. It is possible to find the value of p_∞ (or relative humidity) and (possibly) T_L with the accuracy determined mostly by the accuracy of T_∞. As long as the model is correct it is a method of remote temperature and humidity measurement.

Finally we have investigated in detail the SRT theory of Ward *et al* [23]. According to experimental results and computer simulations the theory needs some revisions. However, it seems to gain accuracy for moderately non-equilibrium processes. In particular SRT does not reduce to (21) which describes correctly the evaporation in single- and multi-component systems.

We conclude that it is indispensable for further progress in the physics of evaporation to run large scale molecular dynamics simulations at equilibrium to determine the evaporation coefficients α_C and α_T and relate them to intermolecular potential and thermodynamic parameters (see recent [102]). These coefficients affect the coefficient P_2 in (21) in the case of evaporation in a single-component system (see also equations (24) and (26)) and also the temperature difference in (26) (and consequently P_1) in the case of evaporation in a multi-component system. They are also important for the description of the smooth transition between the case of evaporation into the vapour of high pressure and the evaporation into vacuum, where it has been exactly shown [26, 27] that $\alpha_C = 2$ in (13). The current paradigm in science is focused on states rather than processes themselves, but most certainly the future belongs to the latter. We hope that our manuscript can guide future studies in this direction.

Acknowledgments

This work was supported by the Ministry of Science and Higher Education/European Science Foundation (ESF/PESC EPSD program) as a scientific project 2010–2013 and by the Polish Ministry of Science and Higher Education under grant no N N202 126837. We would also like to acknowledge the useful discussions with Piotr Flatau on the evaporation of oceans. We also acknowledge discussions with Charles Ward on SRT and the temperature jump at the interface.

Reference

[1] Roderick M L, Hobbins M T and Farquhar G D 2009 Pan evaporation trends and the terrestrial water balance: II. Energy balance and interpretation *Geography Compass* **3** 761–80

[2] Sazhin S S 2006 Advanced models of fuel droplet heating and evaporation *Prog. Energy Combust. Sci.* **32** 162–214

[3] Valero F P J, Collins W D, Pilewskie P, Bucholtz A and Flatau P J 1997 Direct radiometric observations of the water vapor greenhouse effect over the equatorial pacific ocean *Science* **275** 1773–6

[4] Penman H L 1947 Evaporation in nature *Rep. Prog. Phys.* **11** 366–88

[5] Seto J, Tomine K, Wakimizu K and Nishiyama K 2011 Artificial cloud seeding using liquid carbon dioxide: comparisons of experimental data and numerical analyses *J. Appl. Meteor. Climatol.* **50** 1417–31

[6] Wheeler T D and Stroock A D 2008 The transpiration of water at negative pressures in a synthetic tree *Nature* **455** 208–12

[7] Sorensen J G and Holmstrup M 2011 Cryoprotective dehydration is widespread in arctic springtails *J. Insect Physiol.* **57** 1147–53

[8] Chaker M and Meher-Homji C B 2011 Gas turbine power augmentation: parametric study relating to fog droplet size and its influence on evaporative efficiency *J. Eng. Gas Turbines Power* **133** 092001

[9] Singh G, Pillai P, Arpanaei A and Kingshott P 2011 Layer-by-layer growth of multicomponent colloidal crystals over large areas *Adv. Funct. Mater.* **21** 2556–63

[10] Dragnevski K I, Routh A F, Murray M W and Donald A M 2010 Cracking of drying latex films: an ESEM experiment *Langmuir* **26** 7747–51

[11] Dragnevski K I and Donald A M 2008 An environmental scanning electron microscopy examination of the film formation mechanism of novel acrylic latex *Colloids Surf.* A **317** 551–6

[12] Dessler A E and Sherwood S C 2009 A matter of humidity *Science* **323** 1020–21

[13] Fang G and Ward C A 1999 Temperature measured close to the interface of an evaporating liquid *Phys. Rev.* E **59** 417–28

[14] Pao Y-P 1971 Application of kinetic theory to the problem of evaporation and condensation *Phys. Fluids* **14** 306–12

[15] Pao Y-P 1971 Temperature and density jumps in the kinetic theory of gases and vapors *Phys. Fluids* **14** 1340–6

[16] Pao Y-P 1973 Temperature and density jumps in the kinetic theory of gases and vapors *Phys. Fluids* **16** 1560

[17] Cipolla J W Jr, Lang H and Loyalka S K 1974 Kinetic theory of condensation and evaporation: II *J. Chem. Phys.* **61** 69–77

[18] Bedaux D, Hermans L F and Ytrehus T 1990 Slow evaporation and condensation *Physica A: Stat. Mech. Appl.* **169** 263–80

[19] Young J B 1991 The condensation and evaporation of liquid droplets in a pure vapour at arbitrary knudsen number *Int. J. Heat. Transfer* **34** 1649–61

[20] Maxwell J C 1879 On stresses in rarefied gases arising from inequalities of temperature *Phil. Trans. R. Soc. Lond.* **170** 231–56

[21] Persad A H and Ward C A 2010 Statistical rate theory examination of ethanol evaporation *J. Chem. Phys.* B **114** 6107–16

[22] Bond M and Struchtrup H 2004 Mean evaporation and condensation coefficients based on energy dependent condensation probability *Phys. Rev.* E **70** 061605

[23] Ward C A and Fang G 1999 Expression for predicting liquid evaporation flux: statistical rate theory approach *Phys. Rev.* E **59** 429–40

[24] Das K S, MacDonald C A and Ward B D 2010 Stability of evaporating water when heated through the vapor and the liquid phases *Phys. Rev.* E **81** 036318

[25] Hołyst R and Litniewski M 2008 Heat transfer at the nanoscale: evaporation of nanodroplets *Phys. Rev. Lett.* **100** 055701

[26] Hołyst R and Litniewski M 2009 Evaporation into vacuum: mass flux from momentum flux and the hertz–knudsen relation revisited *J. Chem. Phys.* **130** 074707

[27] Cheng S, Lechman J B, Plimpton S J and Grest G S 2011 Evaporation of Lennard-Jones fluids *J. Chem. Phys.* **134** 224704

[28] Babin V and Hołyst R 2005 Evaporation of a sub-micrometer droplet *J. Phys. Chem.* B **109** 11367–72

[29] Babin V and Hołyst R 2005 Evaporation of a thin liquid film *J. Chem. Phys.* **122** 024713

[30] Ward C A and Stanga D 2001 Interfacial conditions during evaporation or condensation of water *Phys. Rev.* E **64** 051509

[31] Maxwell J C 1890 *Collected Sci. Papers* **11** 625

[32] Sirignano W A 2010 *Fluid Dynamics and Transport of Droplets and Sprays* (Cambridge: Cambridge University Press)

[33] Hirschfelder J O, Curtiss C F and Bird R B 1954 *Molecular Theory of Gases and Liquids* (New York: Wiley)

[34] Fukuta N and Myers M N 2007 Simultaneous measurement of condensation and thermal accommodation coefficients for cloud droplet growth in due consideration of a new moving surface-boundary effect *J. Atmos. Sci.* **64** 955–68

[35] Fuchs N A 1959 *Evaporation and Droplet Growth in Gaseous Media* (London: Pergamon)

[36] McGaughey A J H and Ward C A 2002 Temperature discontinuity at the surface of an evaporating droplet *J. Appl. Phys.* **91** 6406–15

[37] Friedlander S K 2000 *Smoke, Dust and Haze Fundamentals of Aerosol Dynamics* (New York Oxford: Oxford University Press)

[38] Pruppacher H R and Klett J D 1997 *Microphysics of Clouds and Precipitation* (Dordrecht: Kluwer)

[39] Jakubczyk D, Zientara M, Kolwas K and Kolwas M 2007 Temperature dependence of evaporation coefficient for water measured in droplets in nitrogen under atmospheric pressure *J. Atmos. Sci.* **64** 996–1004

[40] Landry E S, Mikkilineni S, Paharia M and McGaughey A J H 2007 Droplet evaporation: a molecular dynamics investigation *J. Appl. Phys.* **102** 124301

[41] Walther J H and Koumoutsakos P 2001 Molecular dynamics simulation of nanordoplet evaporation *J. Heat Transfer* **123** 741–8

[42] Langmuir I J 1915 The dissociation of hydrogen into atoms: II. Calculation of the degree of dissociation and the heat of formation *J. Am. Chem. Soc.* **37** 417–58

[43] Zientara M, Jakubczyk D, Kolwas K and Kolwas M 2008 Temperature dependence of the evaporation coefficient of water in air and nitrogen under atmospheric pressure: study in water droplets *J. Phys. Chem.* A **112** 5152–8

[44] Smith J D, Cappa C D, Drisdell W S, Cohen R C and Saykally R J 2006 Raman thermometry measurements of free evaporation from liquid water droplets *J. Am. Chem. Soc.* **128** 12892–8

[45] Knudsen M 1950 *The Kinetic Theory of Gases: Some Modern Aspects* (London: Methuen)

[46] Nathanson G M, Davidovits P, Worsnop D R and Kolb C E 1996 Dynamics and kinetics at the gas–liquid interface *J. Phys. Chem.* **100** 13007–20

[47] Bagot P A J, Waring C, Costen M L and McKendrick K G 2008 Dynamics of inelastic scattering of oh radicals from reactive and inert liquid surfaces *J. Phys. Chem.* C **112** 10868–77

[48] Drisdell W S, Cappa C D, Smith J D, Saykally R J and Cohen R C 2008 Determination of the evaporation coefficient of D_2O *Atmos. Chem. Phys.* **8** 6699–706

[49] McFeely F R and Somorjai G A 1972 Studies of vaporization kinetics of hydrogen-bonded liquids *J. Phys. Chem.* **76** 914–8

[50] Frezzotti A, Gibelli L and Lorenzani S 2005 Mean field kinetic theory description of evaporation of a fluid into vacuum *Phys. Fluids* **17** 012102

[51] Carey V P and Wemhoff A P 2004 Relationships among liquid–vapor interfacial region properties: predictions of a thermodynamic model *Int. J. Thermophys.* **25** 753–86

[52] Ford I J and Lee T-L 2001 Entropy production and destruction in models of material evaporation *J. Phys. D: Appl. Phys.* **34** 413–7

[53] Bellomo N and Chiadò Piat M G 1975 Liquid droplets vaporization gas beam conditions *Meccanica* **10** 57–60

[54] Winkler P M, Vrtala A, Wagner P E, Kulmala M, Lehtinen K E J and Vesala T 2006 Condensation of water vapor: experimental determination of mass and thermal accommodation coefficients *J. Geophys. Res.* **111** D19202

[55] Li Y Q, Davidovits P, Shi Q, Jayne J T, Kolb C E and Worsnop D R 2001 Mass and thermal accommodation coefficients of H_2O (g) on liquid water as function of temperature *J. Phys. Chem.* A **105** 10627–34

[56] Winkler P M, Vrtala A, Wagner P E, Kulmala M, Lehtinen K E J and Vesala T 2004 Mass and thermal accommodation during gas-liquid condensation of water *Phys. Rev. Lett.* **93** 75701

[57] Hagen D E, Schmitt J, Trublood M, Carstens J, White D R and Alofs D J 1989 Condensation coefficient measurement for water in the UMR cloud simulation chamber *J. Atmos. Sci.* **46** 803–16

[58] Zagaynow V A, Nuzhny V M, Cheeusova T A and Lushnikov A A 2000 Evaporation of water droplet and condensation coefficient: theory and experiment *J. Aerosol Sci.* 31 (Suppl.) **1** S795–6

[59] Sageev G, Flagan R C, Seinfeld J H and Arnold S 1986 Condensation of water on aqueous droplets in the transition regime *Colloid Interface Sci.* **113** 421–9

[60] Gollub J P, Chabay I and Flygare W H 1974 Laser heterodyne study of water droplet growth *J. Chem. Phys.* **61** 2139–44

[61] Shaw R A and Lamb D 1999 Experimental determination of the thermal accommodation and condensation coefficients of water *J. Chem. Phys.* **111** 10659–63

[62] Xue H, Moyle A M, Magee N, Harrington J Y and Lamb D 2005 Experimental studies of droplet evaporation kinetics: validation of models for binary and ternary aqueous solutions *J. Atmos. Sci.* **62** 4310–26

[63] Davis E J 2006 A history and state-of-the-art of accommodation coefficients *Atmos. Res.* **82** 561–78

[64] Marek R and Straub J 2001 Analysis of the evaporation coefficient and the condensation coefficient of water *Int. J. Heat Mass Transfer* **44** 39–53

[65] Eames L W, Marr N J and Sabir H 1997 The evaporation coefficient of water: a review *Int. J. Heat and Mass Transfer* **40** 4522–9

[66] Davidovits P *et al* 2004 Mass accommodation coefficient of water vapor on liquid water *Geophys. Res. Lett.* **31** L22111

[67] Kirchner W, Welter F, Bongartz A, Kames J, Schweighoefer S and Schurath U 1990 Trace gas exchange at the air/water interface: measurements of mass accommodation coefficients *J. Atmos. Chem.* **10** 427–49

[68] Rudolf R, Vrtala A, Kulmala M, Vesala T and Wagner P E 2000 Experimental study of sticking probabilities for condensation of nitric acid-water vapor mixtures *Aerosol Sci.* **32** 913–32

[69] Schwartz S E and Freiberg J E 1981 Mass-transport limitation to the rate of reaction of gases in liquid droplets: application to oxidation of SO_2 in aqueous solutions *Atmos. Environ.* **15** 1129–44

[70] Shi Q, Davidovits P, Jayne J T, Worsnop D R and Kolb C E 1999 Uptake of gas-phase ammonia: I. Uptake by aqueous surfaces as a function of ph *J. Phys. Chem.* A **103** 8812–23

[71] Worsnop D R, Zahniser M S, Kolb C E, Gardner J A, Watson L R, Van Doren J M, Jayne J T and Davidovits P 1989 Temperature dependence of mass accommodation of SO_2, and H_2O_2 on aqueous surfaces *J. Phys. Chem.* **93** 1159–72

[72] Jayne J T, Duan S X, Davidovits P, Worsnop D R, Zahniser M S and Kolb C E 1991 Uptake of gas-phase alcohol and organic acid molecules by water surfaces *J. Phys. Chem.* **95** 6329–36

[73] Kolb C E *et al* 2010 An overview of current issues in the uptake of atmospheric trace gases by aerosols and clouds *Atmos. Chem. Phys.* **10** 10561–605

[74] Heideger W J and Boudart M 1962 Interfacial resistance to evaporation *Chem. Eng. Sci.* **17** 1–10

[75] Lednovich S L and Fenn J B 1977 Absolute evaporation rates for some polar and nonpolar liquids *AIChE J.* **23** 454–9

[76] Tsurata T, Kato Y, Yasunobu T and Masuoka T 1994 Estimation of condensation coefficient by dropwise condensation method: condensation coefficients of ethylene glycol and water *Trans. Japan Soc. Mech. Eng.* B **60** 508–14

[77] Maa J R 2001 Rates of evaporation and condensation between pure liquids and their own vapors *Indust. Eng. Chem. Fundam.* **9** 283–7

[78] Chekmarev S F 1996 Effect of condensation heat on the condensation coefficient *AIChE J.* **42** 2467–75

[79] Narusawa U and Springer G S 1975 Measurement of evaporation rates of water *J. Colloid Interface Sci.* **50** 392–5

[80] Jakubczyk D, Kolwas M, Derkachov G, Kolwas K and Zientara M 2012 Evaporation of micro-droplets: the 'radius-square-law' revisited *Acta Phys. Polon.* A **122** 709–16

[81] Viswanathan R, Lakshmi Narasimhan T S and Nalini S 2009 Vapor pressure measurements by mass loss transpiration method with a thermogravimetric apparatus *J. Phys. Chem.* B **113** 8362–8

[82] Price D M 2001 Volatilisation, evaporation and vapour pressure studies using a thermobalance *J. Therm. Anal. Calorimetry* **64** 315–22

[83] Major F G, Gheorghe V N and Werth G 2005 *Charged Particle Traps* (Berlin: Springer)

[84] Davis E J, Buehler M F and Ward T L 1990 The double-ring electrodynamic balance for microparticle characterization *Rev. Sci. Instrum.* **61** 1281–8

[85] Arnold S 1991 A three-axis spherical void electrodynamic levitator trap for microparticle experiments *Rev. Sci. Instrum.* **62** 3025–8

[86] Allison E E and Kendall B R F 1996 Cubic electrodynamic levitation trap with transparent electrodes *Rev. Sci. Instrum.* **67** 3806–12

[87] Dehaeck S and van Beeck J P A J 2008 Multifrequency interferometric particle imaging for gas bubble sizing *Exp. Fluids* **45** 823–31

[88] Zientara M, Jakubczyk D, Derkachov G, Kolwas K and Kolwas M 2005 Simultaneous determination of mass and thermal accommodation coefficients from temporal evolution of an evaporating water microdroplet *J. Phys. D: Appl. Phys.* **38** 1978–83

[89] Jakubczyk D, Derkachov G, Do Duc T, Kolwas K and Kolwas M 2010 Coefficients of evaporation and gas phase diffusion of low-volatility organic solvents in nitrogen from interferometric study of evaporating droplets *J. Phys. Chem.* A **114** 3483–8

[90] Wilms J 2005 *Evaporation of Multicomponent Droplets PhD Thesis* Universität Stuttgart

[91] Ni P 2010 A fuel droplet vaporization model in a hot air stream *Appl. Math. Modelling* **34** 2370–6

[92] Delle Site A 1997 The vapor pressure of environmentally significant organic chemicals: a review of methods and data at ambient temperature *J. Phys. Chem. Ref. Data* **26** 157–93

[93] Lugg G A 1968 Diffusion coefficients of some organic and other vapors in air *Anal. Chem.* **40** 1072–7

[94] The MEGlobal Group of Companies 2005 *Diethylene Glycol Product Guide* www.meglobal.biz/media/product_guides/MEGlobal_DEG.pdf

[95] Duan F, Thompson I and Ward C A 2008 Statistical rate theory determination of water properties below the triple point *J. Phys. Chem.* B **112** 8605–13

[96] The International Association for the Properties of Water and Steam. *Revised Release on the IAPWS Formulation 1985 for the Thermal Conductivity of Ordinary Water Substance*. London, England, 1998

[97] Vrabec J, Kedia G K, Fuchs G and Hasse H 2006 Comprehensive study on vapour-liquid coexistence of the truncated and shifted lennard-jones fluid including planar and spherical interface properties *Mol. Phys.* **104** 1509–27

[98] Long N L, Micci M M and Wong B C 1996 Coefficients of evaporation and gas phase diffusion of low-volatility organic solvents in nitrogen from interferometric study of evaporating droplets *Comput. Phys. Commun.* **96** 167

[99] Consolini L, Aggarwal S K and Murad S 2003 A molecular dynamics simulation of droplet evaporation *Int. J. Heat Mass Transfer* **46** 3179–88

[100] Allen M P and Tildesley D J 1987 *Computer Simulations of Liquids* (Oxford: Oxford University Press)

[101] Resibois P and de Leener M 1977 *Classical Kinetic Theory of Fluids* (New York: Wiley)

[102] Ishiyama T, Yano T and Fujikawa S 2005 Kinetic boundary condition at a vapor-liquid interface *Phys. Rev. Lett.* **95** 084504